Tectonophysics 906 (2025) 230722

Contents lists available at ScienceDirect

Tectonophysics

journal homepage: www.elsevier.com/locate/tecto

Dyke emplacement and its interaction with fracture systems and regional stress fields: Combination of a field study and geochronology in Cserhát Hills, Hungary

Dorina Juhász [a,b,c,*], Chiara Lanzi [d,e], Zsolt Benkó [a,f], Freysteinn Sigmundsson [d], Barbara Beke [b], Françoise Bergerat [g], László Fodor [h,b]

[a] Institute for Nuclear Research, Bem tér 18/c, 4026 Debrecen, Hungary
[b] Eötvös Loránd University, Institute of Geography and Earth Sciences, Department of Geology, Pázmány Péter sétány 1/c, 1117 Budapest, Hungary
[c] Karlsruhe Institute of Technology, Institute of Applied Geosciences – Structural Geology and Tectonics, 76131 Karlsruhe, Adenauerring 20a, Germany
[d] Nordic Volcanological Center, Institute of Earth Sciences, University of Iceland, 101 Reykjavík, Sturlugata 7, Iceland
[e] Icelandic Meteorological Office, Reykjavik, Iceland
[f] Department of Mineralogy and Geology, University of Debrecen, 4032 Debrecen, Egyetem tér 1, Hungary
[g] Sorbonne Université, CNRS–INSU, Earth Science Institute of Paris, UMR 7193, 4 place Jussieu, 75252 Paris Cedex 05, France
[h] HUN–REN Institute of Earth Physics and Space Science, Csatkai E. utca 6–8, 9400 Sopron, Hungary

ARTICLE INFO

Keywords:
Dyke emplacement
Volcanism
Stress field
Fault–slip analysis
Pannonian Basin

ABSTRACT

Widespread andesitic volcanism with several eruption centres occurred during the Middle Miocene in the Cserhát Hills, central – northern Hungary. In this time, an extensive dyke system developed in the area, where some dykes have exposed maximum length of 23 km, and maximum width of 25 m. This dyke system shows a change in its strike from E–W to NNW–SSE. Here we integrate new and previous field observations to derive structural maps and study dykes and fractures in the Cserhát Hills. K/Ar geochronology is used to understand the temporal evolution of regional fault patterns before, during and after the formation of the dykes and also to gain insights into the interaction between the dyke emplacement and the regional stress field. Fault-slip data were collected at 27 different sites along the dykes and were combined with reinterpreted datasets from 16 sites located at a distance from dykes. The field observations, integrated with the geochronological data sets suggests that dykes with different orientations were emplaced in two different eruptive cycles around 15.4 and 14.7 Ma. The deformation history of the Pannonian Basin involved a clockwise change in regional minimal stress axis, probably as a result of regional vertical–axis counter-clockwise block rotation. Our field observations suggest strike-slip stress regime may occur near propagating dyke tips, and the direction of minimal stress axis may have locally rotated counter-clockwise where dykes changed their strikes and emplaced along pre-existing fractures, mostly normal faults.

1. Introduction

Studies of dyke emplacement and propagation have been an important research theme since the first half of last century (e.g., Anderson, 1937, 1951; Delaney et al., 1986; Guðmundsson, 1984). In the last few decades such studies have been conducted to understand dyke dynamics and associated seismic and volcanic hazards (e.g., Drymoni et al., 2021; Greiner et al., 2023; Guðmundsson, 2006; Guðmundsson, 2002; Guðmundsson and Brenner, 2004; Heimisson et al., 2015; Shukla et al., 2022; Sigmundsson et al., 2015). Vertical to sub-vertical, steeply dipping dykes, inclined sheets, and sub-horizontal sills can propagate laterally as well as vertically (Heimisson et al., 2015; Maccaferri et al., 2016). Dyke propagation is an important mode of magma transport that may lead to a volcanic eruption, if it reaches the surface. The propagation path and dyke arrest can be influenced by many different factors, for example, topography (Heimisson et al., 2015; Sigmundsson et al., 2015), crustal stress regimes and tectonic stress (e.g., Sigmundsson et al., 2024), faulting coeval with dyke emplacement (Drymoni et al., 2020, 2021; Greiner et al., 2023; Maccaferri et al., 2016), and changes in lithology of host rock (Guðmundsson and

* Corresponding author at: Institute for Nuclear Research, Bem tér 18/c, 4026 Debrecen, Hungary.
E-mail address: dorina.juhasz@kit.edu (D. Juhász).

https://doi.org/10.1016/j.tecto.2025.230722
Received 18 May 2024; Received in revised form 26 March 2025; Accepted 28 March 2025
Available online 29 March 2025

Brenner, 2004; Schmiedel et al., 2021).

The pathway of a dyke is facilitated by extensional stress and pre-existing faults (Anderson, 1951; Stephens et al., 2018). In addition to opening on dyke planes, the modelling of Stephens et al. (2018) suggests furthermore that shearing across dykes may also be common in an extensional domain. Dyke emplacement depends on regional stress trajectories, as well as tectonic stress gradients, buoyancy and length of fractures (Dahm, 2000). If this statement is true, dyke orientation can be used for stress axes estimation (Anderson, 1937; Hou et al., 2010). Regional stress fields can be perturbed near volcanic centers, and in such places dyke orientation can be radial away from volcanic centers (Anderson, 1937; Guðmundsson, 1995; Rivalta et al., 2015), or off-rift volcanism can occur (Maccaferri et al., 2014; Mazzarini et al., 2016). The orientation of dykes is not always fully perpendicular to the direction of least compressive stress, in particular when dykes form along previously formed fractures. This has been observed e.g., in Iceland both in extinct eroded volcanoes (Greiner et al., 2023) and in recent dyke injections (e.g., Ruch et al., 2016). Furthermore, Daniels and Menand (2015) used analogue modelling to show that dyke orientation in repeated injections into the same area can depend on the ratio of dyke overpressure versus pre-existing tectonic stress that may evolve significantly during repeated dyke injections.

A segmented, km-scale, andesitic system of dykes is found in the Cserhát-Nógrád area, Hungary (Noszky, 1940; Póka et al., 2004). This dyke system is connected to widespread Miocene volcanism of the Pannonian Basin (Harangi, 2001; Karátson, 2007; Harangi et al., 2024) and propagated more than 18 km away from volcanic centers. The dykes exhibit a notable variation in strike direction, shifting from E-W in the south to NNW-SSE in the north. Additionally, strike changes are also observed within individual dykes. The study area was influenced by several brittle deformation phases with progressively changing palaeostress axes predating or synchronous with the rifting of the Miocene Pannonian Basin. These phases led to formation of normal faults and associated grabens trending from WNW–ESE to NNE–SSW (Noszky, 1940; Benkovics, 1991; Csontos, 1995; Fodor et al., 1999; Soós, 2017). The dyke system might have interacted with these structures.

The dyke system at the Cserhát Hills has not been studied before in detail in terms of (i) the emplacement mechanisms and (ii) the connection to the governing stress field. In this study, we investigate the nature and evolution of the dyke system with combination of different field observations, including measurements of fractures (dip direction, dip angle, strike), dyke geometry (length and width), and host rock-dyke interactions. Our geochronological data gives new constraints on the age of different magma emplacement events and helps to date changes in the regional stress field. The revised and temporally well-constrained regional stress field data helps to better understand the dynamics of the dyke system, including the relationships between the regional stress regime and the orientation of the dykes, and their possible interaction with pre-existing structures (e.g., faults) in the study area.

2. Geological background

2.1. Regional tectonic setting

The Cserhát Hills are situated in the central-northern region of Hungary, in the northern part of the Pannonian Basin. This area is also part of the Inner Carpathian volcanic arc of Miocene age (Fig. 1a). Extension in the back-arc Pannonian Basin was driven by inferred roll-back subduction associated with mantle flow (Horváth et al., 2015). The rifting followed a Paleogene to earliest Miocene contractional basin formation period (Fodor et al., 1992; Tari et al., 1993) which resulted in the formation of NE-trending folds, minor thrusts, and a major ENE-trending dextral strike-slip zone, the Mid-Hungarian Shear Zone (MHSZ, Fig. 1b, Csontos and Nagymarosy, 1998; Ruszkiczay-Rüdiger et al., 2007, 2009; Palotai and Csontos, 2010). The transition from contraction to rifting occurred roughly around 19–18 Ma and is marked by the filling of the contractional basin and the onset of extension-related new subsidence phase.

Several events of counter-clockwise vertical-axis rotations occurred during the syn-rift phase, carefully documented by palaeomagnetic methods (Márton and Márton, 1996; Márton and Pécskay, 1998; Márton et al., 2007a, 2007b). The consequence of block rotation is evident in the stress field evolution, as changes in the direction of the principal stress axes in clockwise direction have been reported in the same time period as the counter-clockwise rotations occurred (Márton and Fodor, 1995). The change in stress field activated or deactivated extensional or transtensional faults with different orientations and has permitted the separation of several syn-rift events within the entire syn-rift deformation process (Fodor, 2011; Petrik et al., 2016). The extensional episodes are reflected in km long faults of variable orientations and dominated by faults of NW– SE and N–S to NNE–SSW direction, documented already in early mapping projects (Hámor, 1985), local and regional fault analyses both on the surface and subsurface (Benkovics, 1991; Bada et al., 1996; Csontos, 1995; Nemčok and Lexa, 1990; Oláh et al., 2014; Tari et al., 1992; Vass et al., 1993), and basin-wide fault-slip analyses (Bergerat et al., 1984; Csontos et al., 1991; Fodor et al., 1999). During the rifting the MHSZ (Fig. 1b) remained active, playing a role of transfer fault (Tari et al., 1992) with a sinistral kinematics during the late stage of evolution (Palotai, 2013; Petrik, 2016; Petrik et al., 2016).

Active magmatism in this area occurred from the late Early to early Middle Miocene (Karpatian – Badenian stages, 17.2–12.8 Ma; for local Paratethys stages see Kováč et al., 2017) and was driven by the convective upwelling of the asthenosphere and extension of the lithosphere inducing decompressional melting (Harangi and Lenkey, 2007; Lukács et al., 2021). Several widespread pyroclastic explosions can be traced across the basin and serve for correlation (Eger-Ipolytarnóc, Tihamér, Tar, and Harsány formations, Lukács et al., 2022; Karátson et al., 2022). The study area is marked by the Mátra Andesite Complex (Harangi, 2001; Póka et al., 2004; Karátson, 2007; Gál and Lukács, 2024), which is composed of complex andesitic volcanic edifices, shallow intrusions, and a segmented dyke system. The timing of the magmatism in the Cserhát Hills coincides with the syn-rift phase of the Pannonian Basin (Fodor et al., 1999; Harangi, 2001; Horváth et al., 2015). Thus, the magmatism was coeval with the two rotation events (Márton and Márton, 1996; Fodor et al., 1999).

2.2. Stratigraphy

Paleogene to earliest Miocene sediments of the Cserhát Hills deposited in the so-called North Hungarian-South Slovak Paleogene Basin, a retroarc contractional basin related to subduction process below the Carpathians (Báldi and Báldi-Beke, 1985; Tari et al., 1993). Parts of the infilling clastic sedimentary rocks exhibit similar lithology, consisting primarily of poorly lithified sandstone or siltstone (“schlier” in the local terminology) (Fig. 2a). The most common basin-filling are the Szécsény Schlier, Pétervására, Budafok, and the Törökbálint Sandstone formations, that are typical marine formations of the Paleogene to early Miocene basin (Báldi, 1986; Sztanó, 1994, 1995; Sztanó and Tari, 1993) (see the ages in million years on Fig. 2a).

The syn-rift sequence starts with terrestrial clastics (Zagyvapálfalva Formation). The first pyroclastic rocks cover the terrestrial clastics or older formations. The pyroclastics mainly occur north and north-east of the Cserhát Hills (Tihamér Formation on Fig. 2a). The age of the Tihamér Formation is now well-constrained as 17.4 Ma (Karátson et al., 2022; Lukács et al., 2021). Fast subsidence in the syn-rift graben occurred in the late Early Miocene (Fig. 2, e.g., Salgótarján Brown Coal, Egyházasgerge, and Fót formations, Hámor, 1985; Püspöki et al., 2017; Sóron, 2011). Dyke swarm can be found in all of these pre–Middle Miocene formations. East from the exposed dyke system deltaic to marine Middle to Upper Miocene sediments fill the Zagyva Graben system. The potential westward extension of this graben filling sediments was eroded from above the dykes during Plio–Quaternary uplift (Dunkl and

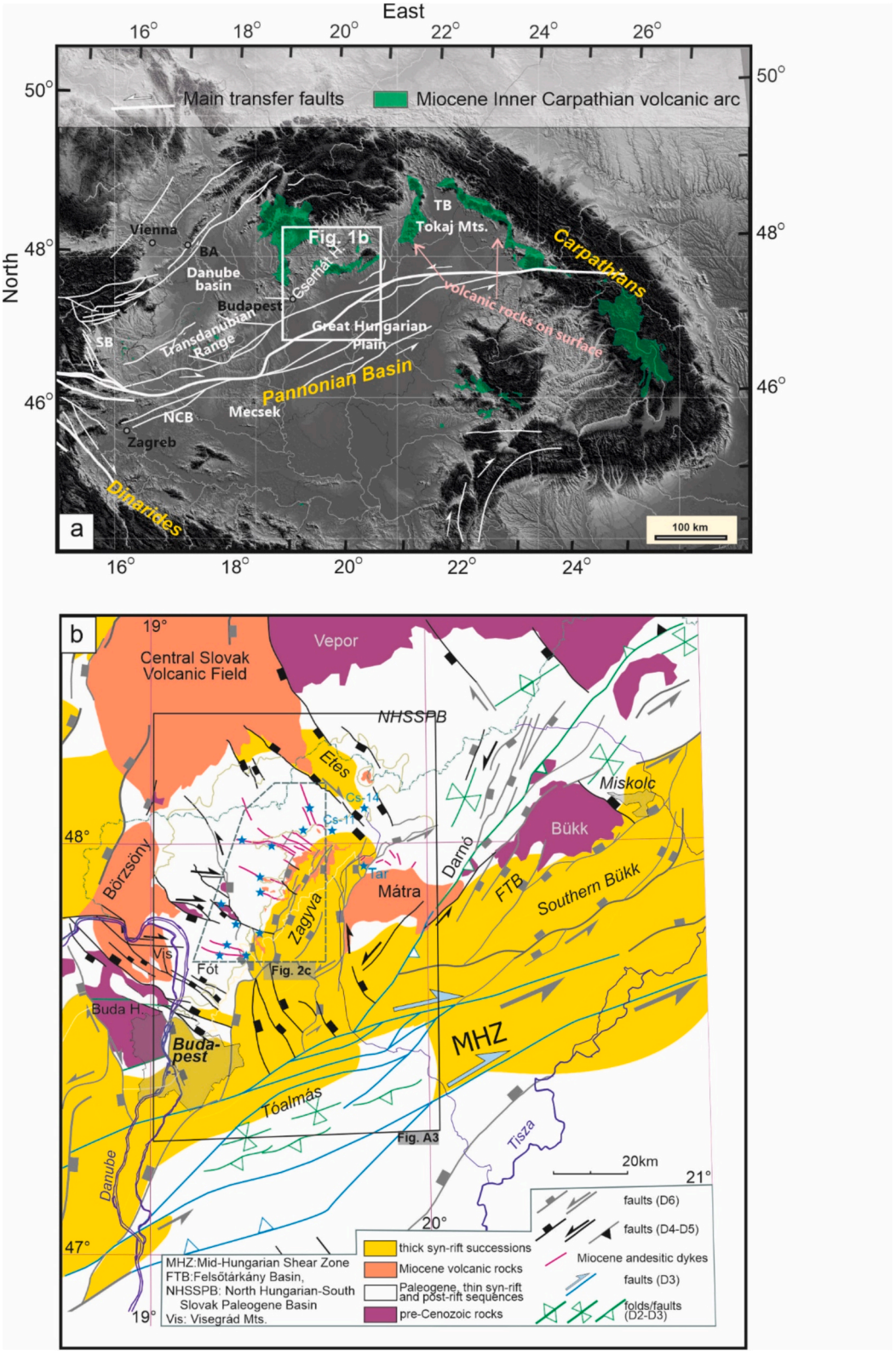

Fig. 1. Regional setting and stratigraphy of the studied area, the coordinates are in WGS 84: (a) The location of the Cserhát Hills within the Pannonian Basin with respect to the Carpathian orogenic arc, the Miocene to Quaternary volcanic arc. BA: Bratislava, TB: Transcarpathian Basin, SB: Styrian Basin, NCB: North Croatian Basin. Modified after Lukács et al. (2018) (b) Faults in northern Hungary that played a role during the pre-rift contractional-strike-slip phases (D2 – D3) and several *syn*-rift phases (D4 – D6). Modified after Fodor et al. (1999); Fodor (2011); Petrik et al. (2016); Beke et al. (2019). Blue stars mark the location of fault-slip measurements of in this study, see details on Figs. 2, and A6 marked by grey frame. (For interpretation of the references to colour in this figure legend, the reader is referred to the web version of this article.)

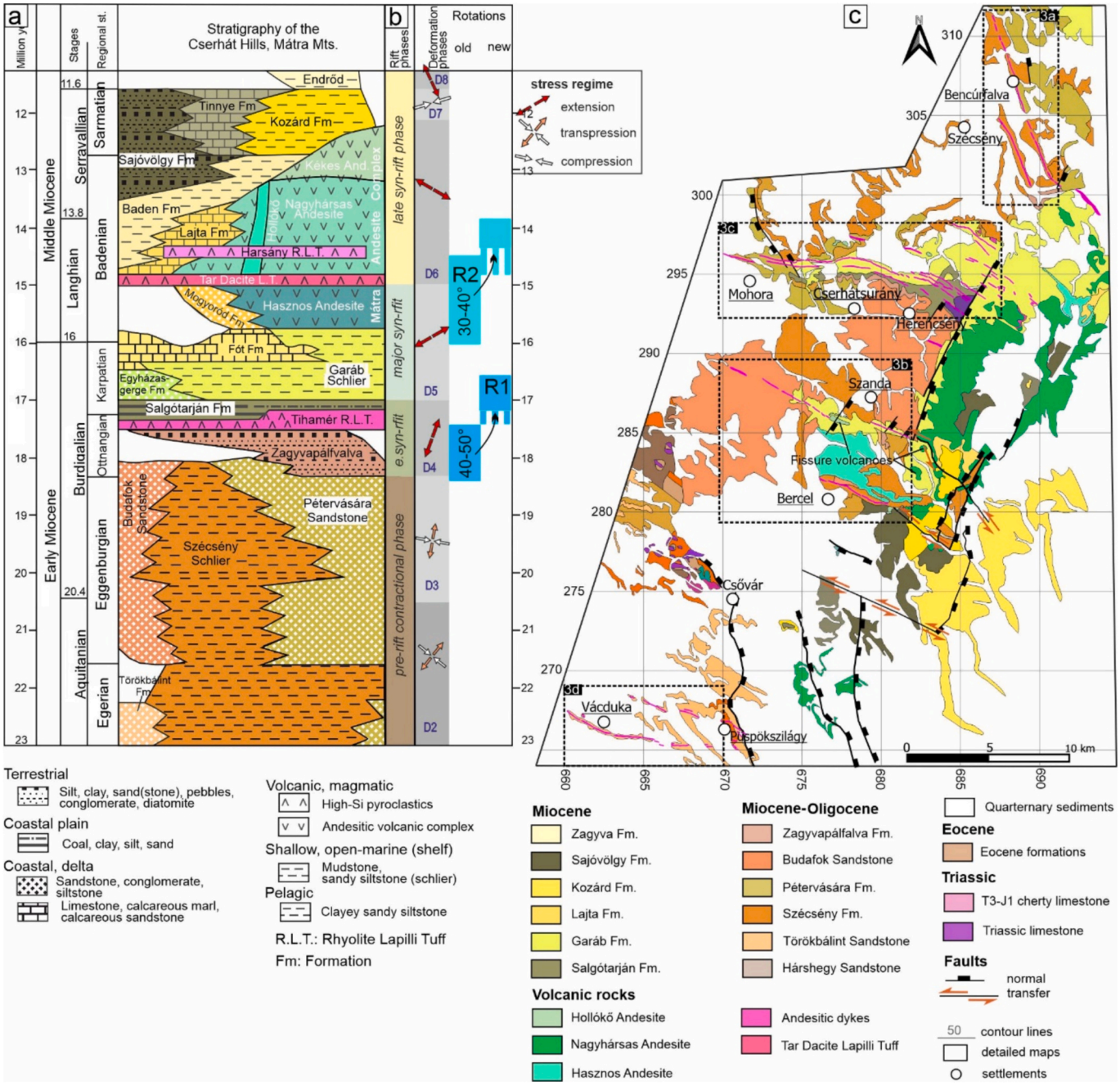

Fig. 2. Stratigraphy and deformation phases: a) Stratigraphic column of the study area (modified after Selmeczi et al., 2024; Lukács et al., 2022; Gál and Lukács, 2024). The Tihamér Formation partly corresponds to the "Eger-Ipolytarnóc Member" of Karátson et al. (2022), the Tar Formation to the "Játó Member" of Biró et al. (2020). b) Major basin-forming phases, deformation phases based on fault-slip analyses, and the timing of rotations. Note old and new versions for time spans of rotations (Márton and Pécskay, 1998, versus this study). c) Geological map of the study area (modified after Gyalog and Síkhegyi, 2005; Hámor, 1985; Noszky, 1940; Soós, 2017). The pink lines (long and thin polygons) are the dykes. Dashed frames show the location of detailed maps in Figs. 4–5. (For interpretation of the references to colour in this figure legend, the reader is referred to the web version of this article.)

Frisch, 2002).

Volcanic rocks in the study area, which belong to the dyking events, are part of different lithological units of the extensive Mátra Andesite Complex (Gál and Lukács, 2024; Karátson, 2007). The attribution of dykes to different units is ambiguous because of the close temporal relationship and large errors in former K/Ar geochronological data (Pécskay et al., 2006). The Hasznos Volcanosediment, likely produced during the interval of ~16–14.9 Ma, is the oldest unit of the Mátra Volcanic Complex (Gál and Lukács, 2024; Hámor, 1985). Borehole stratigraphy confirms their thickness of several hundred metres (Hámor, 1985). An unpublished report on the southern Cserhát Hill (Püspökszilágy area) attributed some dykes to this rock unit (Budai et al., 2005). The Tar Dacite Lapilli Tuff Formation is a key horizon of few tens to 120 m thickness and is well dated as 14.9 Ma (Lukács et al., 2018); but its mapped extent is minor in the study area.

Most of the rock units of the Mátra Andesite Complex overlie the Tar Formation (Fig. 2). The younger part of the Mátra Andesite Complex is built up by several andesitic formations, including the Nagyhársas, Hollókő, and Kékes andesites. The Nagyhársas Andesite, a significant volcanic rock in the eastern Cserhát Hills, is characterised by explosive pyroclastic rocks and vesicular pyroxene andesite lava flows. Although the older K/Ar ages indicate a wide time span for its formation

(16.3–14.5, Pécskay et al., 2006; Póka et al., 2004), the andesite complex is always above the Tar Formation, thus should be younger than ~14.9 Ma. According to earlier views of Póka et al. (2004) some dykes, mainly near Szanda and Bercel, belong to this unit. The Kékes Andesite, representing the closing phase of volcanic activity is estimated to be 13.5–11.0 Ma old (Gál and Lukács, 2024; Karátson, 2007). The recently defined Hollókő Andesite (Gál and Lukács, 2024) comprises the dykes of the Cserhát Hills with suggested K/Ar age of 15.0–13.5 My (Pécskay et al., 2006; Póka et al., 2004). It has been suggested that the dykes in the northern Cserhát belong to this unit or to the Nagyhársas, and Kékes andesites (Gál and Lukács, 2024; Gyalog and Síkhegyi, 2005; Póka et al., 2004).

2.3. Evolution of the stress field

The Miocene stress field evolution of the Pannonian Basin (later referred to as PB) and surrounding Alpine orogens was highly influenced by rotation of crustal blocks. In fact, this part of the PB was affected by counterclockwise (CCW) rotations (Márton and Fodor, 1995). The maximum compressional stress (σ_1) had initially direction close to E–W during the Paleogene to earliest Miocene (D2 and D3 phases, see in Fig. A1), but then gradually occupied all positions up to ~NE–SW during the CCW rotations (Fig. 2b; Fodor et al., 1999). This corresponds to the regional phases D4–D6 as defined by Petrik et al. (2016) and Beke et al. (2019) (Fig. 2b, and Fig. A1).

The first CCW rotation of about 45–50°, referred to as R1, occurred around 18.5–17.5 Ma considering time constraints from geochronological data of rotated volcanic and sedimentary rocks (Márton and Pécskay, 1998; Márton et al., 2007a, 2007b). However, more recent data permitted to locate the rotation to a period between 17.4 and 16.8 Ma, within the early part of the syn-rift phase (Fig. 2b) (Lukács et al., 2015, 2018, 2021). Estimates of timing the second CCW rotation, referred to as R2, amounting to 30–40° are somewhat different. Márton and Pécskay (1998) and Márton et al. (2007b) indicated a time span between 16.0 and 14.5 Ma, while new data indicate ~14.8–14.0 Ma. Irrespective of bias in their timing, both rotations, R1 and R2, occurred during the peak of extension and magmatism.

Detailed analyses based on field observations demonstrated that rotation of the stress axes continued after the vertical-axis rotations; near the turn of Middle to Late Miocene the maximal horizontal stress axis (σ_{Hmax}) may have been ENE–WSW (Phase D7 and D8, Petrik et al., 2016, Fig. 2b). During the late syn-rift and post-rift stages, (D9 phase; Petrik et al., 2016) extension direction rotated back to ENE–WSW.

3. Methods

3.1. Structural mapping and fault-slip data analysis

Structural mapping was undertaken in the central and southern Cserhát Hills, focusing particularly on the geometric features of dykes, including their strikes, thickness and length, and the fracture pattern within and near the dykes, to understand better the interaction between the dykes and faults. We also used an unpublished structural map in the southern Cserhát Hills (Püspökszilágy area, Budai et al., 2005). During the field work we measured fractures (faults with or without striae, joints, cooling joints, and veins) within and in proximity (from tens to-, hundreds of metres) to the dykes as well as dip of host sedimentary strata. Field data was recorded by Field Move software (https://www.petex.com/pe-engineering/move-suite/digital-field-mapping/), and subsequently visualised on stereoplots using the InnStereo (https://innstereo.github.io/) software.

The field data helped us to estimate the palaeostress fields that were active before and after the dyke emplacement. For minimum palaeostress axis estimation we followed the model of Anderson (1951) and selected conjugate pairs of shear fractures in addition to tensional ones. For striated faults we used the software of Angelier (1984) for stress tensor calculation. Selection of kinematic groups was executed by automatic phase separation module of Angelier and Manoussis (1980) and also manually, following the approach of (Fodor, 2011). To enhance the robustness of our dataset, a comparative analysis was conducted by juxtaposing our findings with existing fault-slip datasets available from the study area or wider surroundings (Beke, 2016; Beke et al., 2019; Benkő and Fodor, 2002; Benkovics, 1991; Fodor et al., 1999; Márton and Fodor, 1995; Petrik et al., 2016; Vass et al., 1993; Vojtko et al., 2019). Preexisting field data were gathered from 1986 to 2015. We reinterpreted all relevant data to achieve homogeneously analysed fault-slips and palaeostress database. Reactivation of earlier conjugate fracture set by oblique-slip faulting, the relative chronology of fractures and bed tilting, and other criteria were used to establish succession of fracturing phases. During this process, we started with published faulting chronology, but the analyses resulted in a refined history. The interpreted data are summarised in Fig. A1 and Tables A1-A3. Using these structural data, a simplified pre–Quaternary geological map was constructed (Fig. A3). This is based on published maps, unpublished works, and fault-slip data sets (Noszky, 1940; Fusán and Zoubek, 1964; Wein, 1977; Hámor, 1985; Prakfalvi et al., 2005a, 2005b, 2005c; Rónai et al., 2005; Soós, 2017).

3.2. K/Ar dating

Andesite dykes of different orientations (NNW–SSE, Location CSER22–18 and WNW–ESE, location CSER22–09) were selected and sampled for K/Ar dating (Fig. 3 and Table A3). Dated sites are shown on Fig. 3 and Fig. A3. Careful sampling was carried out on the field, in order to avoid altered or weathered samples which may suffer unwanted argon or potassium loss. Samples were crushed, sieved, and washed ultrasonically. Based on the average phenocrysts grain size, the 63–125 mm fraction was selected for further separation by heavy liquid and magnetic separator. To avoid excess Ar carried by mafic phases, plagioclase and groundmass fractions were isolated using sodium– polytungstate heavy liquid, with density ranges, typically 2.58–2.65 g/cm^3 and < 2.65–2.70 g/cm^3, respectively. The residual mafic phases were removed by Frantz magnetic separator.

The pure mineral fractions were dated at the Geochronology Lab of the Institute for Nuclear Research (Debrecen, Hungary) using the unspiked K-Ar method, following the procedure of Cassignol and Gillot (1982) and Gillot and Cornette (1986). Potassium contents were measured on 50 mg sample aliquots, after dissolution with HF and HNO_3, using a Sherwood-400-type flame spectra-photometer with accuracy better than ±1 %. Potassium analyses are routinely compared to the HD-B1 (Hess and Lippolt, 1994), ISH-G and MDO-G (Gillot et al., 1992) standards. Separated mineral sample aliquots were then heated at 100 °C for 24 h under vacuum, to remove atmospheric Ar contamination that was adsorbed onto the surface of the mineral particles during sample preparation. Argon was extracted from the materials by fusing the samples via high-frequency induction heating at 1300 °C. The released gases were cleaned in two steps in a low-blank vacuum system using hot St-101 and cold St-707 getters, respectively. The isotope composition of Ar was measured using an Argus VI© multi-collector noble gas mass spectrometer. The non-spiked procedure renders the knowledge of the exact $^{40}Ar/^{36}Ar$ atmospheric ratio unnecessary. The calibration of our ^{40}Ar signal is checked routinely using analyses of the HD-B1 (Hess and Lippolt, 1994; Schwarz and Trieloff, 2007), BB-6 (Jäger et al., 1985) standards. During the present study, analyses of HD-B1 yielded an age of 24.14 ± 0.34 Ma, which compares well with the recommended values of 24.21 ± 0.32 Ma. Standard BB-6 yielded 0.440 ± 0.007 Ma which differs only insignificantly from the reported 0.441 ± 0.013 Ma age. Decay constants recommended by Steiger and Jäger (1977) were used for the age calculation, with an overall error of ±1 %. Error of the samples was calculated using the equation of Quidelleur et al. (2001).

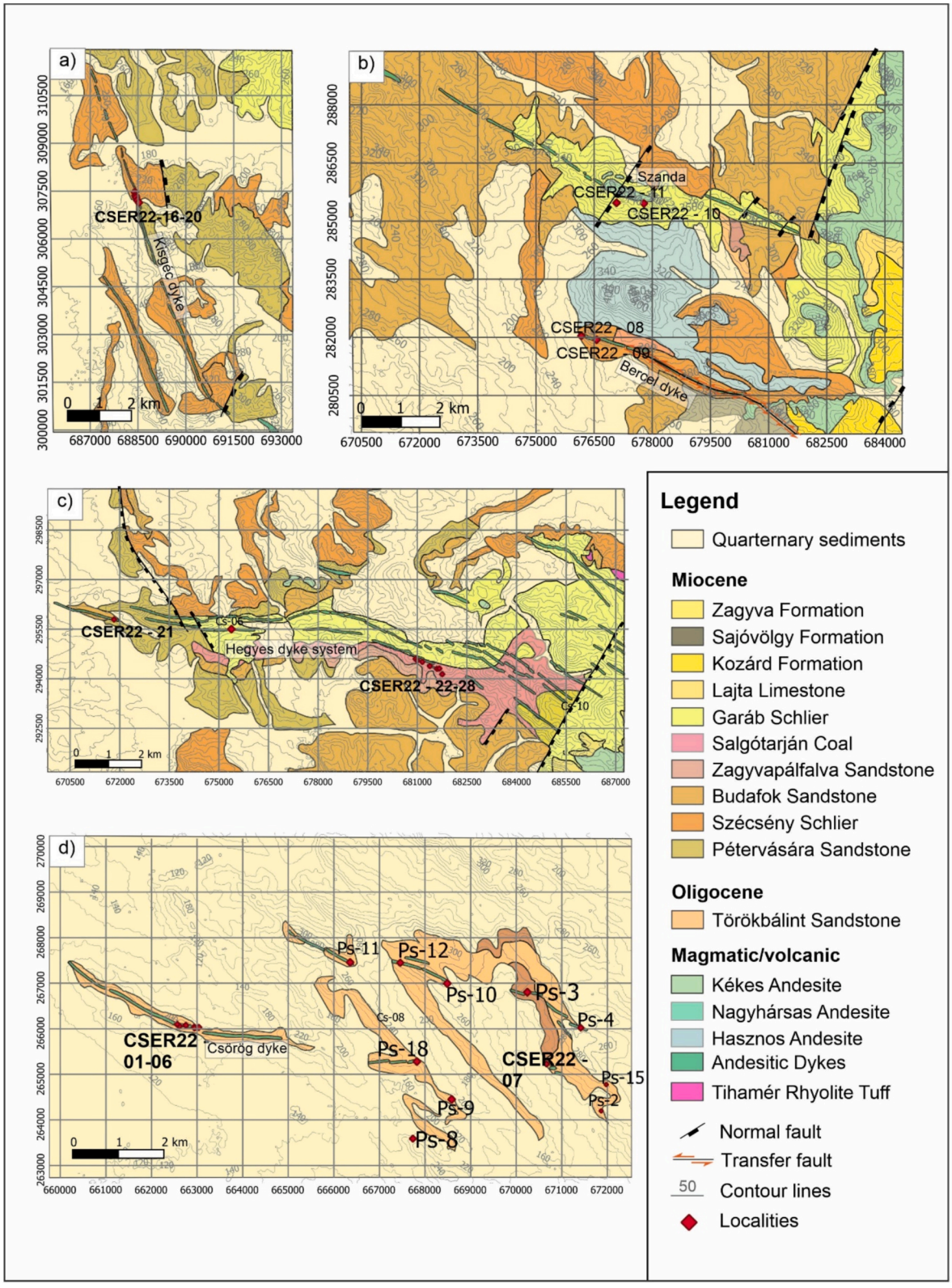

Fig. 3. Geological maps of the neighborhood of four dyke areas, where the dykes are shown by green elliptical polygons (modified after Noszky, 1940; Soós, 2017; Supervisory Authority of Regional Affairs of Hungary). The coordinates are in the Hungarian National Grid EOV in metres. Numbers with a dash in between mean several closely spaced localities: (a) Area of the northern Kisgéc dykes east of Szécsény, near Benczúrfalva (Fig. 2c). Here the dykes have significantly different strike direction than the southern ones. (b) The dykes near Szanda (north) and Bercel (south) (Fig. 2c). According to the map, smaller volcanic centres might have been located here. (c) Area of Mohora (west) and Cserhátsurány (east) (Fig. 2c). The dykes have remarkable changes in their strike. (d) The area of Püspökszilágy (Figs. 2c, 5). (For interpretation of the references to colour in this figure legend, the reader is referred to the web version of this article.)

4. Results

4.1. Structural observations

During the fieldwork in 2022, dyke observations were carried out at 27 locations, where the vegetation made it possible (Fig. 3). At these locations we measured the thickness and length of dykes as well as dip and strike of the dyke and fractures, if they were presented (Table A1). In the past, andesite in the dykes was important raw material used for construction, and most of the dyke material was excavated along narrow and long trenches. In certain locations, excavation of andesite has resulted in deep trenches with collapsed sidewalls, leaving only boulders in the debris as indicators of the dyke's presence. The observed andesites exhibited significant weathering on their surfaces. In most of the sites, the contact between the dyke and the host rock, consisting of Oligocene to Lower Miocene fine-grained clastics, was well-exposed and available for study albeit only in small exposures. The reinterpretation concerned 16 sites, most frequently former quarries, as illustrated on Figs. 3, and A3.

4.1.1. Dyke geometry

Length and thickness are important parameters of a dyke, but we pay particular attention also to along-strike variation and segmentation of dykes. It is necessary to check if the cross-cutting faults, shown almost perpendicular to dyke strike on the former maps (Fig. 2), are real features, or the overlapping segments are interpreted as having been cut across by faults. The best examples are from the southern dykes and the longest Hegyes dyke system in the central-northern part of the study area (Figs. 3d, c respectively, and Fig. A3).

In the southern area, two major dyke sets can be followed: the southern Csörög and the northern János Hill dykes (Noszky, 1940) (Fig. 4). The eastern part of the area, previously mapped by Budai et al. (2005), was now surveyed also by structural geological approach. The mapped dyke segments are located on the crest of long ridges standing out from the morphology (Fig. 5a). Between outcropping segments, the dykes may have subsurface connections while Quaternary deposits cover them (Figs. 3d, and 4).

In the eastern part of the Cserhát Hills, the Paleogene–Early Miocene clastics are covered by a thin syn-rift sequence and then discordantly by Upper Miocene post-rift formations (Fig. 4), possibly indicating the proximity to the base-syn-rift surface at the time of magma emplacement than the more exhumed western part, where the base-syn-rift surface has not been preserved. Sites Ps–4, and Ps–15 (Fig. 3d) expose larger andesite bodies whose oval shape and their mixing with sediments can indicate a near-surface evolution of the volcanism (Budai et al., 2005).

Strike of measured contacts between the dykes and host rocks varies between E–W and NW–SE (between azimuth 080° and 130°) and the alternation of different directions gives a wavy appearance to the dyke sets. Segmentation leads to locally slightly different strike than for of the whole dyke set. In the eastern part of the area, an NNW–striking dyke is inferred but the scattered outcrops can alternatively be interpreted as eroded remnants of surface andesite flows (between sites Ps–4 and Ps–15, Fig. 4).

On the surface, colinear but non-continuous segments occur. One clear example is at site CSER22–01 where a deeper roadcut exposes only the host Oligocene clastics but not the dyke. In contrast, the colinear dyke segments are verified (Fig. 4). Non-colinear steps between dyke segments are frequently present, with both left- and right-stepping continuation occurs. Where stepping direction was consistent for few segments, this resulted in a slight difference in the orientation of the individual segments and the zone of dyke segments (insets of János Hill dyke, sites Ps–10–12, –3, Fig. 4). The width of overlap zone between different dyke segments was on average 20–50 m. The systematic stepping direction suggests that some of the dykes (as reaching to the present surface) were intruded in en-echelon arranged segments, eventually in fractures of a coeval or inherited strike-slip zone. Considering the overlap geometry, the presence of cross faults, as postulated in earlier studies (Noszky, 1940) can be, at least locally, excluded.

On the other hand, curvature of the strike of dykes or branching of shorter side segments are also present. This is quite systematic, the bend is always from E–W to WNW–ESE or up to NW–SE direction, representing a clockwise change if looking toward the tip point of the dyke. One prominent example is from the western end of the Csörög dyke (Figs. 3d and 4) while debranching is also present there.

In the central dyke system, near sites CSER22–08, CSER–09 and CSER22–10, CSER–11 (Bercel and Szanda dyke systems, Figs. 3b and

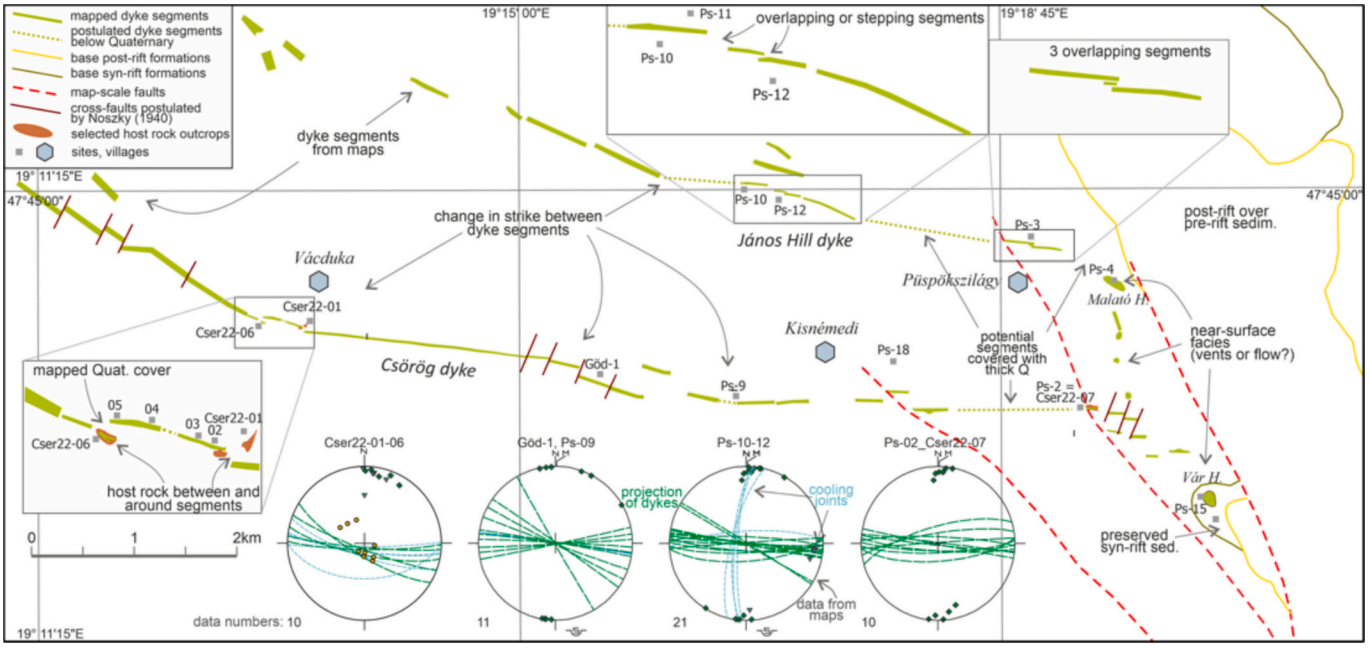

Fig. 4. Geometry of dyke segments, and measured field data (Schmid stereonet, lower hemisphere projection) in the southern Cserhát Hills. See the geological map on Fig. 3d. Note 3-fold magnification of overlapping dyke segments in critical regions shown in detail. Faults are after Budai et al. (2005). For detailed legend of the stereonets see Fig. 6.

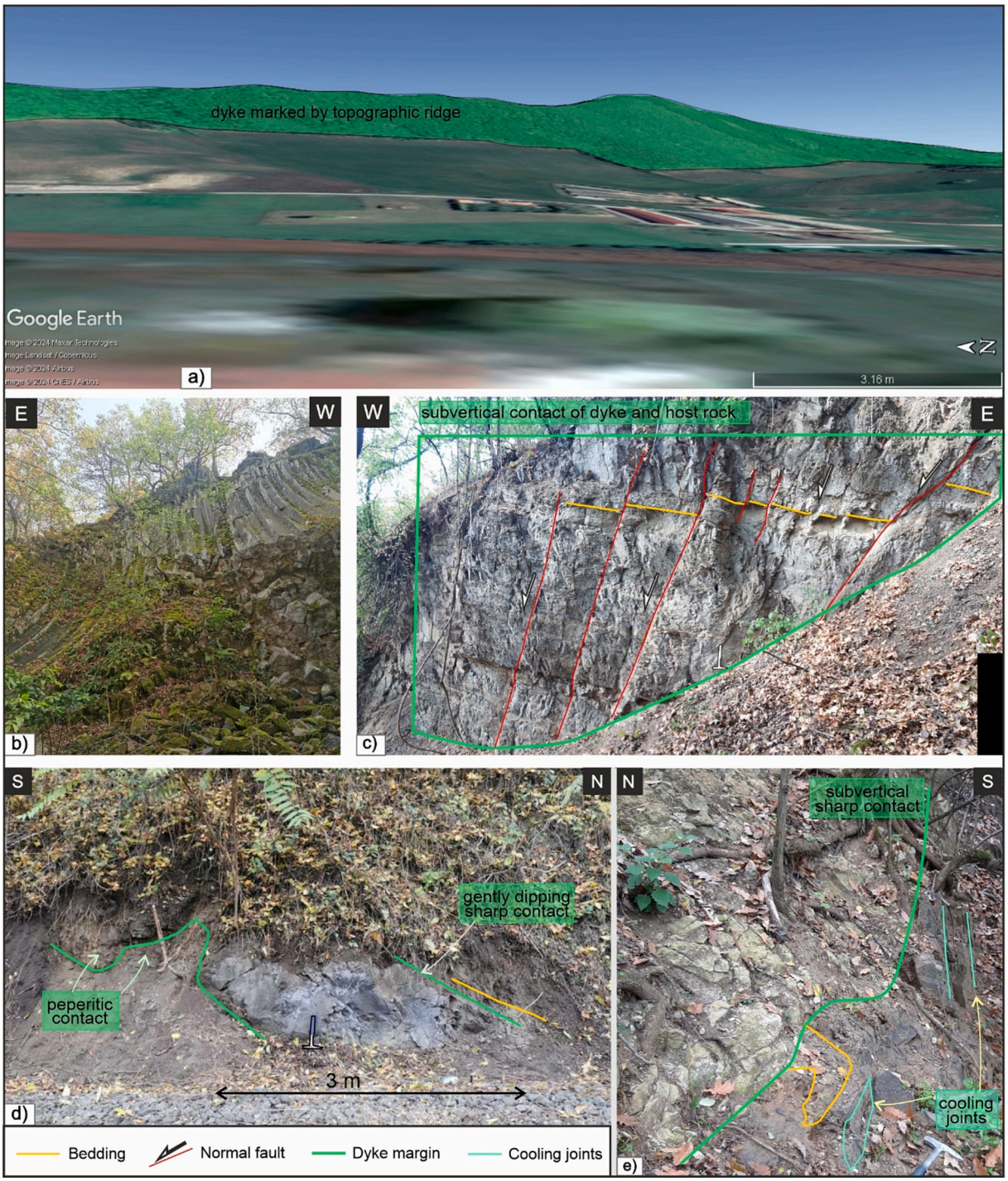

Fig. 5. Morphological, structural and magmatic features of dykes and host rocks in some outcrops of the Cserhát Hill. (a) Oblique aerial view of a dyke segment near Bercel (close to CSER22–08 and CSER22–09), using Google Earth. The dyke is outstanding in form of a ridge due to selective Quaternary denudation process. (b) Hexagonal columnar andesite near Bér indicating near-surface development. (c) Normal faults, shown by red lines (F4 set) crossing the subvertical contact of the eastern end of the Csörög dyke, site CSER22–07, Ps-02. (d) Inclined andesite sheet and its contacts near the western end of the main Hegyes dyke in site CSER22–21. Peperite marks the original moderate dip of dyke margins. (e) Sub-vertical contact of andesite dyke segment of the Hegyes dyke system, site CSER22–23. Note small protrusions of host rocks in d) and e). Note hammer for scale. (For interpretation of the references to colour in this figure legend, the reader is referred to the web version of this article.)

A3), near surface volcanic facies are present in the form of small bodies, similarly to the southern dyke set. These andesite bodies are connected to the central Szanda and the Hegyes dyke systems. The andesite bodies, and several dykes intrude already the oldest syn-rift clastics at their preserved shallowest parts. Curved hexagonal columns are present at these locations (Fig. 5b). According to Hetényi et al. (2012), dykes can form columnar joints, with columns perpendicular to the magma flow.

At the Hegyes dyke system, the dyke orientation is variable but similar to the southern system. The Hegyes dykes have north–westerly strike in the east, then display mostly an E–W trend in its central segment while few debranching segments turn to NW at the western dyke part and appear on the surface in Slovakia (Figs. 1b, 3c, and A6).

Balla (1989) interpreted the E–W dyke segment as a sign for sinistral displacement of originally NW–SE striking dykes; however, no such displacement in the order of 10 km is detectable in other stratigraphical or structural markers. Thus, we consider this geometry as magmatic one.

Along the longest Hegyes dyke system, we studied the central part and its western termination. At CSER22–21, the margin of a narrow dyke

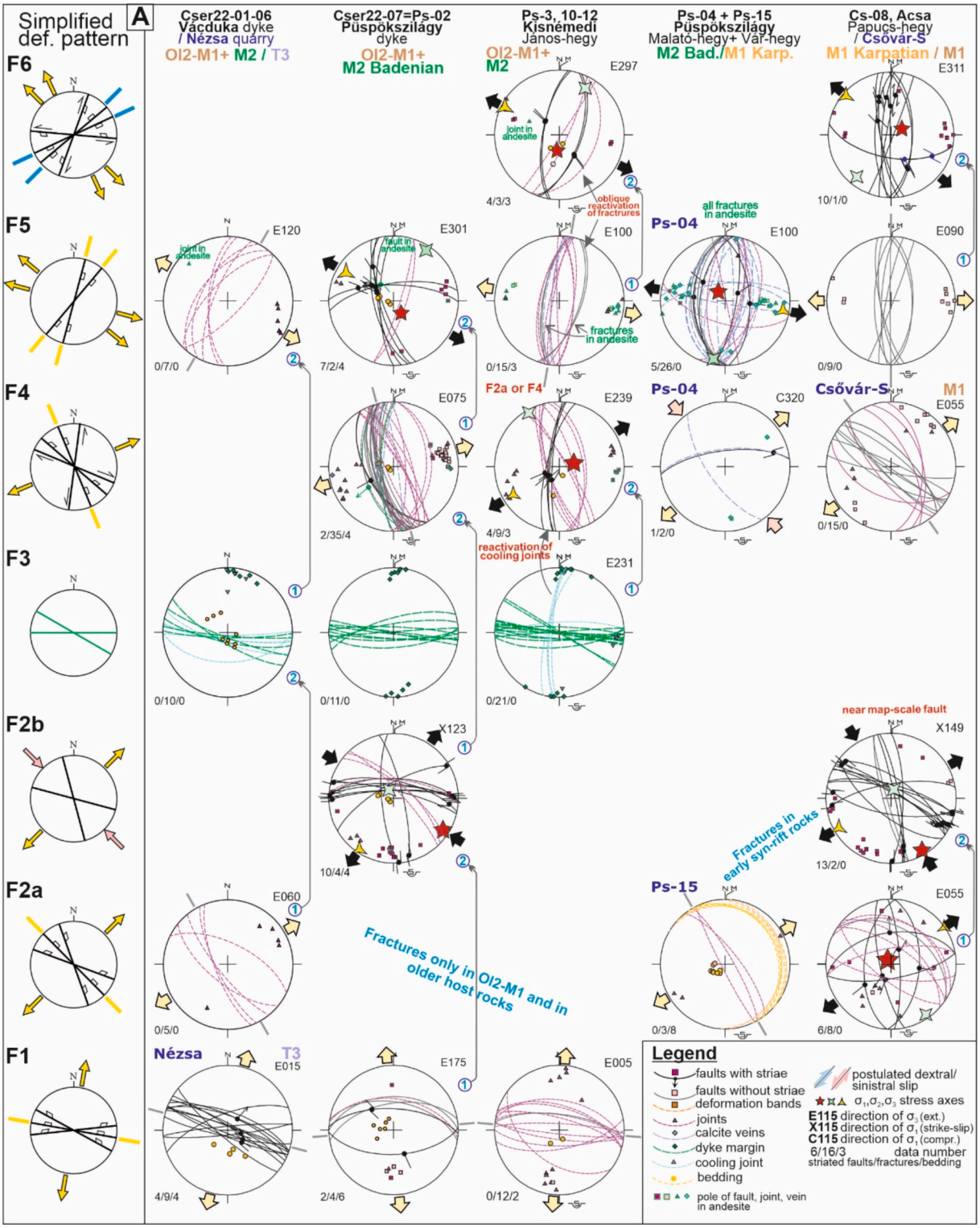

Fig. 6. Fracture sets calculated or estimated stress axes, and relative chronology for measured structural data, and the proposed simplified fault pattern and stress axes (left column) in the (a) southern Cserhát, and (b) in the central to northern Cserhát Hills. The data from the 2022 field campaign are presented together with data from older measurements. Some columns show a single locality, while others contain data from different sites. (See locations of sites on Fig. 1, Fig. 4). Def.: deformation, Bad.: Badenian, Karp.: Karpatian. Further abbreviations: T3: Late Triassic, Ol2-M1: Late Oligocene – Early Miocene, M2: Middle Miocene. Grey arrows with blue numbers indicate relative chronology. (For interpretation of the references to colour in this figure legend, the reader is referred to the web version of this article.)

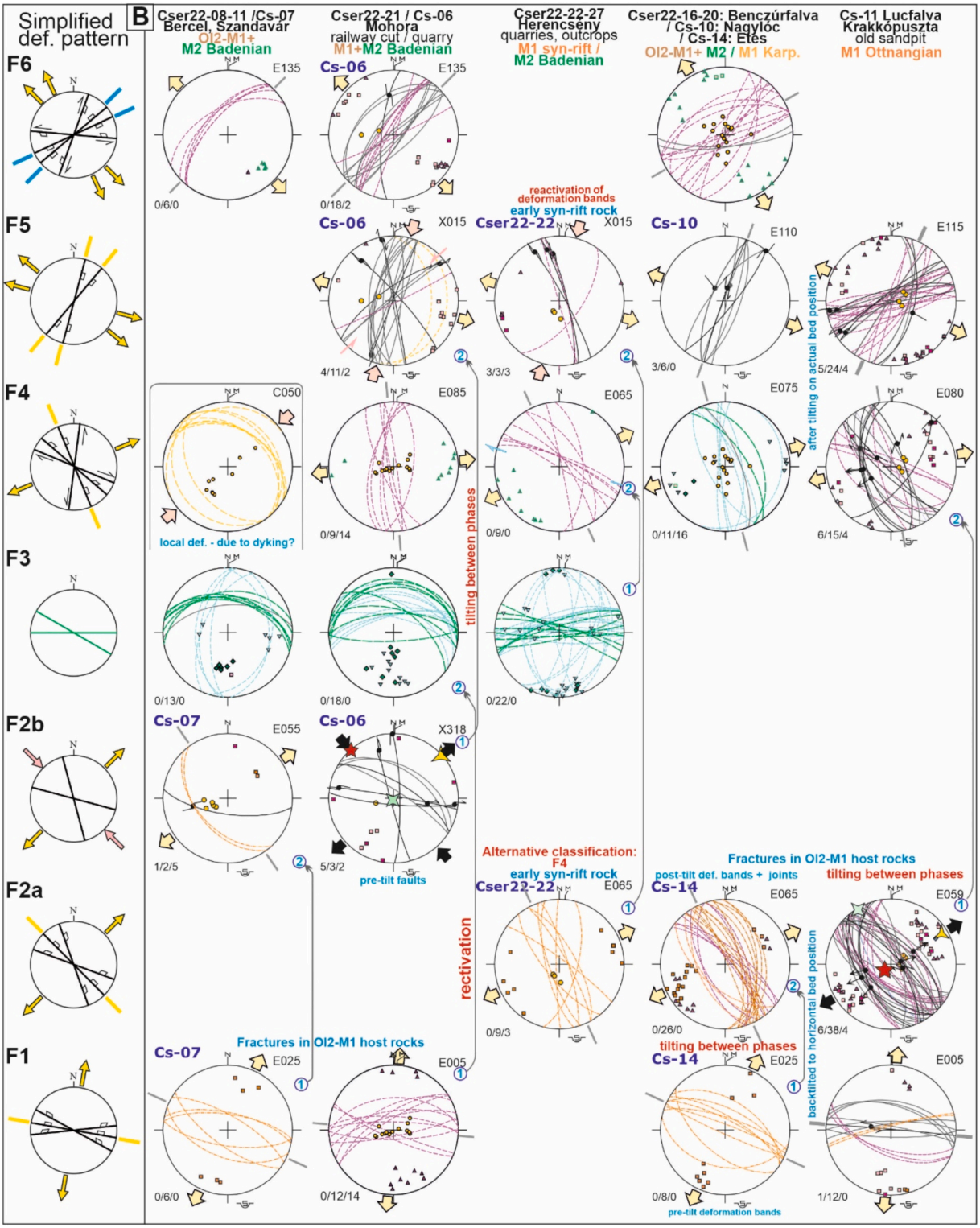

Fig. 6. (*continued*).

segment is exposed with a marked peperitic transition at the contact with the host rock (Fig. 5d). The measured moderate dip of the margin suggests that this is in fact an inclined andesitic sheet dipping to the north (Fig. 6). Near sites CSER22–22, CSER22–23, CSER22–24, CSER22–25, CSER22–26, and CSER22–27, we walked out 7 different segments of a dyke system (Fig. 5e). Direct measurements of dyke margin surfaces are varying between E–W and WNW–ESE, this latter direction reflects the map view of dykes (Fig. 6). Unfortunately, Quaternary cover impeded the observation of the continuity or overlapping nature of the exposed segments.

The northernmost Kisgéc dyke system starts with short segments with SE–NW strike in the south–east than the main part is NNW–SSE oriented; few shorter parallel dykes associate the main one. (Figs. 3a, and A3). Outcrops were larger and of better quality compared to most locations. The strike of the detected dyke margin aligned with one set of the cooling joints, showing ENE–WSW extension, while the other set is

perpendicular to the first (Fig. 6). This dyke system is parallel to the northern branch diverging from the Hegyes dykes (Fig. 2b). On the other hand, the SE end of the Kisgéc dykes form about 1.5 km bend or step and a similar step can be seen on the base–syn-rift stratigraphic horizon; the presence of a pre-, or post-dyke fault cannot be excluded (Fig. A3). Further to the SE, within the syn-rift sequence, few intrusive bodies can be suspected but their relationship to the Kisgéc dykes is hidden.

4.1.2. Fault-slip data

All the measured structural data are plotted on stereograms, shown in Fig. 6a, b. Searching for Andersonian type conjugate fractures (Anderson, 1937, 1951) seven fracture sets were separated both in the southern and central–northern part of the Cserhát Hills using the approach described in the Methods chapter. F1 fracture set of E–W striking faults and shear joints correspond to N-S extension, and it was measured only in Oligocene to earliest Miocene siltstones predating the formation of the dyke (Fig. 6). At the sites of Nézsa, CSER22–07, Ps–3–10–12, CSER22–21, and Cs–11 (Figs. 3b, d) this set is represented by discrete fracture planes (faults and joints) while in pre-rift porous sandstones deformation bands were formed (Cs–07, Cs–14, Fig. A3). These deformation bands in Cs–07 (Bercel) are the earliest fracture set formed at a shallow burial position, close to deposition of the sand (Beke et al., 2019). Similarly trending map-scale faults mainly occur near the Mesozoic horsts, like Naszály, Romhány (Fig. A3)

F2a and F2b fracture sets were formed in extensional and strike-slip regimes, respectively (sites CSER22–01–06, Ps–15, Cs–08, CSER22–23–27, Cs–14, Cs–11, and sites CSER22–07, Cs–08. Cs–07, 06, respectively, Figs. 3, and A3). These stress states share the NE–SW oriented minimum principal stress axis. NW–trending normal faults, joints and veins belong to the extensional regime, while E–W trending dextral and conjugate N-S trending sinistral faults are part of the strike-slip regime. All these fractures appear in rocks older than the dykes. Examples from the study area include dextral faults in the Miocene Visegrád Complex, the Naszály and Romhány horsts (Fig. A3). The largest map separation occurs near site Cs-08; it is ~2 km at the base–syn-rift level and supported by local fault-slip data (Fig. A3). At one site of late Early Miocene age (Cs–08 in Fig. 6a), strike-slip faults reactivated pre-existing planes of former normal faults thus F2a set could be older than F2b but this can be only a local relative chronological datum. Site Cs–14 offers a very important relative chronology datum: the observed deformation bands of the F1 fracture set predated the tilting while deformation bands of F2 set followed the tilt deformation (Beke, 2016).

F3 fracture set comprises the dykes themselves, measured along their margins. Except of the northern Cserhát Kisgéc dyke, all other are E–W to NW–SE trending. The dip values are close to vertical but in site CSER22–21 the moderate dip of the margins and parallel cooling joints argue for an inclined sheet (Figs. 5d, and 6b). In sites Ps–3, −10, −12 and CSER22–08, −09, −10, −11, −22–27 (Fig. 3) cooling joints are perpendicular to the dykes.

F4, F5, F6 fracture sets were formed in extensional regime, where the minimum principal stress σ_3 was oriented ENE–WSW, E–W to ESE–WNW and SE–NW, respectively. These fracture sets appear in map-scale fault pattern at site CSER22–07, the observed outcrop-scale normal faults, veins, joints of NNW–SSE strike (Fig. 5c) are parallel to map-scale faults which cut across the entire stratigraphy (Fig. 4). The postulated NE–striking "cross fault" of Noszky (1940), displacing the dykes, and major faults east of the study area in the Zagyva graben would belong to fracture set F5 (Figs. 1b, and A3). F4 to F6 sets are younger than the dykes, because the dyke material has been involved in these fracturing processes (sites CSER22–01, −07–08, −11, −21–27) or all fractures have affected near-surface andesite bodies (site Ps–04). The separation of these three sets is based on relative chronology and the oblique dextral-normal slip of a younger phase on older fracture planes. F4 is older and reactivated by F5 in site CSER22–07, and F5 is older than F6 in sites Ps–03, −12 and Cs–08 (Fig. 6).

The fracture system at sites CSER22–22–27, displaying the oldest syn-rift sediments (late Early Miocene). It does not contain the F1 E–W striking joints, but only a few NW–SE striking fractures (F2 set) and several deformation bands which are classified either as F2 or as F4 set (Fig. 6). The bands were formed in very shallow burial depth and represent an early fracturing event at the early phase of rifting (Beke et al., 2019). However, their relative timing with respect to dyking cannot be determined. Later, the deformation band surfaces were superimposed by strike-slip striae, having been formed in NNE–SSW compression and ESE–WNW extension (F5 fracture set). The σ_3 axis of this strike-slip stress state is similar to other sites with extensional fractures (where σ_1 axis is vertical) and we consider this case as a permutation of σ_1 and σ_2 axes within the same phase (Angelier and Bergerat, 1983; Hu and Angelier, 2004).

4.2. Geochronological results

The results of the geochronological measurements are shown in Table 1 with their locations indicated in Fig. A3. Groundmass fraction of an andesite dyke with NNW–SSE orientation, sampled at Benczúrfalva ("Kisgéc dyke", 48°06′32"N 19°33′46″E) yielded K/Ar ages from 14.52 Ma to 14.72 Ma. Standard deviation of the groundmass analyses and a single plagioclase age (14.41 ± 0.21 Ma) overlap with each other within one sigma error. The perfectly overlapping ages measured on groundmass and plagioclase indicate no preferential argon loss or addition to the system, the system remained closed. The isochron age of the sample is 14.66 ± 0.58 Ma.

Two separate samples were taken from a WNW–ESE striking, macroscopically fresh andesite dyke at Bercel ("Bercel dyke", 47°52′52.2"N 19°24′19.7″E). K/Ar ages of separated groundmass (15.31 ± 0.22 Ma and 15.21 ± 0.22 Ma) and plagioclase (15.34 ± 0.23 Ma and 15.41 ± 0.22 Ma) fractions overlap with each other within one sigma error. The isochron age of the two samples is 15.39 ± 0.43 Ma. K/Ar age of a whole rock andesite from Hegyes dyke (Hegyes Hill), (48°00′04.9"N 19°27′09.5″E) yielded an age of 15.23 ± 0.22 Ma. The new ages confirm that the older dykes (Bercel, Hegyes, and Csörög) belong to the Hasznos Volcanoclastic Rocks, while the younger dyke set to the Hollókő Andesite, and not to the younger Kékes Andesite.

5. Discussion

5.1. Reliability of ages from the dyke system

Although the correlation between the temporal change of the stress field and the age of the magmatic dykes of the Cserhát Hills has been previously proposed (Márton and Fodor, 1995; Póka et al., 2004), it lacked the complementary investigation with geochronological data of sufficient resolution. NW– to N–striking – magmatic dykes from the eastern Cserhát Hills and the Zagyva graben were suggested to be younger than 13.5 Ma, while in the central and southern Cserhát Hills, a WNW–ESE striking dyke swarm was considered older than 14 Ma. (Póka et al., 2004). The published ages of Póka et al. (2004) are in line with the K/Ar ages of andesites ranging from 13.8 ± 0.8 Ma to 16.0 ± 1.4 Ma (Balogh, 1984). The previous K/Ar geochronological analyses were performed partly on whole rock and partly on mafic mineral fractions (e.g., biotite, amphibole), while plagioclase and matrix fractions were usually skipped due to their possible alteration and preferential Ar-loss. However, according to Lahitte et al. (2019) and Molnár et al. (2022), even the groundmass fraction can give a fully reliable K/Ar age if the sample selection is sufficiently accurate. In addition, the K/Ar age of the groundmass will certainly be free of excess Ar and will provide the age of crystallization of the subvolcanic rock. In our study we combined accurate sample selection and separation, applied the non-spiked K/Ar method and used a multicollector mass spectrometer. This allows us to provide accurate ages for structural analysis and reliably review of the former K/Ar ages inferred by Balogh (1984). In line with the previously observed relative age relationships, the formation of the Kisgéc andesite

Table 1
New K/Ar ages obtained in this study from two different dyke sets. Column headings indicate name of the site location, K/Ar lab code, grain size, dated mineral phase, potassium (K) concentration in percent, concentration of radiogenic (40Arrad) in percent, concentration of radiogenic (40Arrad) in cm^3 at standard temperature and pressure, age ± 1-sigma uncertainty (in Ma).

Sample name	K/Ar lab code	Grain size (μm)	Dated material	K [%]	$^{40}Ar_{rad}$ [%]	$^{40}Ar_{rad} \times 10^{-7}$ [ccSTP/g]	Age [Ma]
Benczúrfalva	9233	63–125	groundmass	1.70	0.35	9.673	14.52 ± 0.21
Benczúrfalva	9233	63–125	groundmass	1.71	0.37	9.681	14.54 ± 0.21
Benczúrfalva	9233	63–125	groundmass	1.71	0.39	9.803	14.72 ± 0.21
Benczúrfalva	9233	63–125	plagioclase	0.48	0.21	2.710	14.41 ± 0.21
Bercel	9234	63–125	groundmass	2.81	0.32	16.801	15.31 ± 0.22
Bercel	9234	63–125	plagioclase	0.45	0.22	2.683	15.34 ± 0.23
Bercel	9235	63–125	groundmass	2.69	0.31	15.958	15.21 ± 0.22
Bercel	9235	63–125	plagioclase	0.42	0.41	2.5490	15.41 ± 0.22
Hegyes Hill	9190	63–125	whole rock	1.65	0.33	8.712	15.23 ± 0.22

dykes in the northern Cserhát Hills (14.66 ± 0.58 Ma) is about ~0.7 Ma younger than the Bercel and Hegyes dykes of the central Cserhát Hills (15.39 ± 0.43 Ma). The age of the Kisgéc dyke is ~1 Ma older than suggested (Póka et al., 2004).

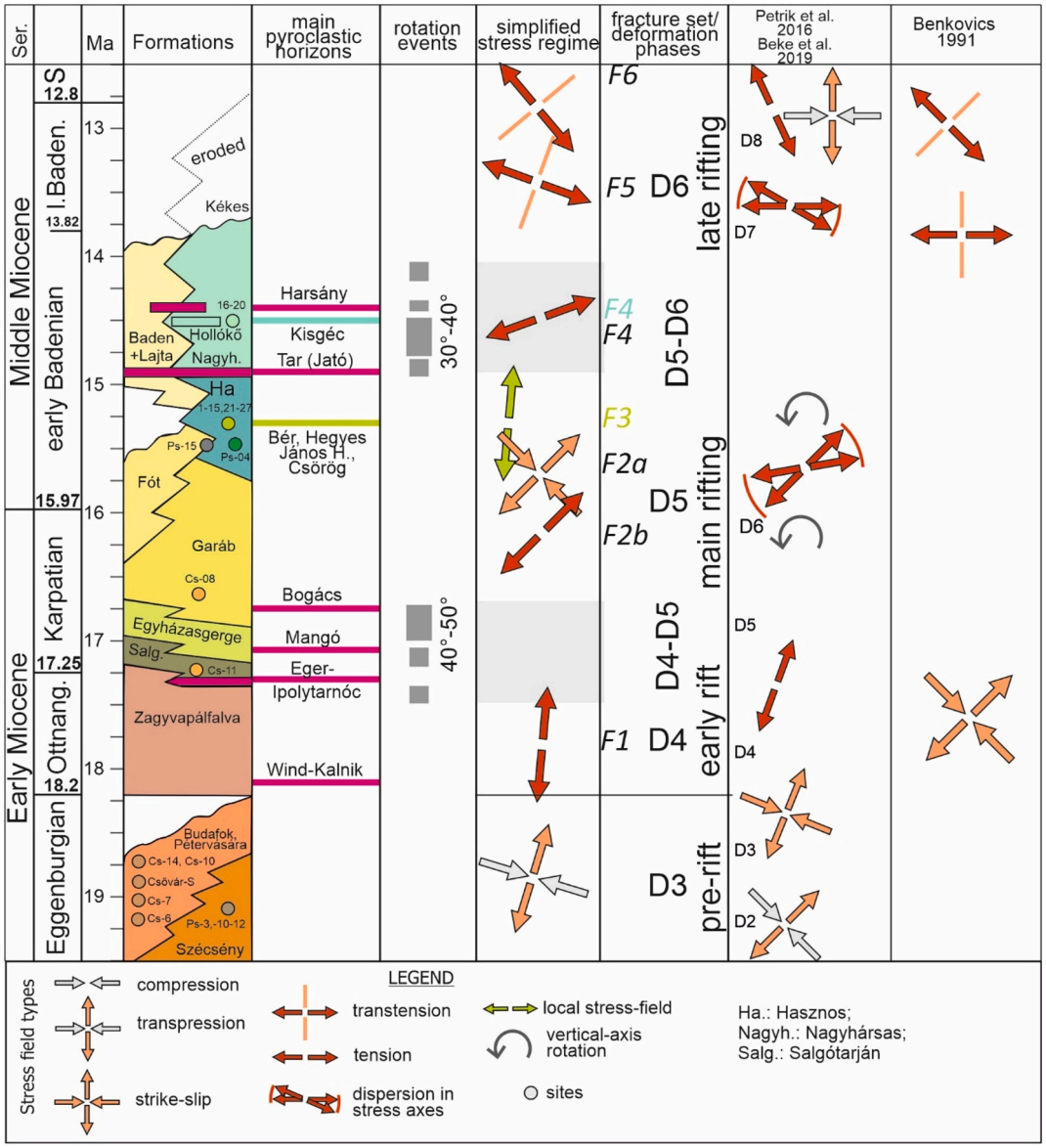

Fig. 7. Correlation of fracture sets, regional stress fields, vertical-axis rotations, and main volcanic horizons. Formations are after Selmeczi et al. (2024), Gál and Lukács (2024), ages of pyroclastic horizons are after Biró et al. (2020); Brlek et al. (2023); Karátson et al. (2022); Lukács et al. (2018, 2021). Time spans of rotations are modified from Márton and Fodor (1995); Márton and Pécskay (1998); and Petrik et al. (2016). Width and continuity of grey columns reflect the certain and probable periods of rotation events. Grey boxes mark the transition between different stress regimes. See a detailed version of comparison of the stress regime on Fig. A1.

5.2. Structural evolution, correlation of stress fields with regional data

5.2.1. Interpretation of field measurements

Seven fracture sets were distinguished in the present study, including, as a separate event, the emplacement of the dykes. Six of them represent different episodes of the rifting process, while the last one may be a part of the post-rift phase. This can be compared to numerous fault-slip analyses performed in the south–western Cserhát Hills (Benkő and Fodor, 2002), in NE Hungary and southern Slovakia (Beke, 2016; Beke et al., 2019; Márton and Fodor, 1995; Petrik et al., 2016; Vass et al., 1993; Vojtko et al., 2019) and in the entire Pannonian Basin (Fodor et al., 1999). The inferred number of phases and their temporal bounds varyfrom study to study, but in general, they can be categorised into pre-, syn-, and post-rift phases (Figs. 7, and A1.).

The first deformation phase observed in this area exhibits a clear N-S directed extension (F1), as evidenced by tectonic joints, faults measured in host rocks of the Csörög, János Hill and Hegyes dykes (CSER22–07, Ps–12, and CSER22–21). The stress field for this phase was calculated only from data measured in pre-rift formations, both during this study and in earlier works (Fig. 7 and Fig. A1). The age of this extension depends on the correlation of the fracture system to the regional tectonic phases. Because in other sites in NE Hungary, the same extensional stress regime was noticed in the earliest *syn*-rift sediments (Cs–11, Fig. 6), we correlate the local F1 fracturing to the regional D4 phase representing the early syn-rift phase (Beke et al., 2019; Petrik, 2016). Older studies did not infer that the ~N–S extension was a separate deformation phase (Benkő and Fodor, 2002; Vass et al., 1993), but either considered it as a local variation of NE–SW extension (Fodor et al., 1999) or regarded it only as a local extensional stress state in a strike-slip regime marked by E–W to ESE–WNW maximal stress axis (Márton and Fodor, 1995) (Fig. A1). In the newest classification the strike-slip regime corresponds to the D3 phase (Fig. 7, Beke, 2016; Petrik et al., 2016). This is a regionally important phase and predated the rifting (Beke, 2016; Beke et al., 2019; Fodor et al., 1999; Palotai, 2013; Petrik et al., 2016) and could characterize the dextral slip along the MHZ (Fig. 1, and Fig. A1). In this study, we emphasize the separate nature of the D3 strike-slip and D4 extensional faulting phases (following Petrik et al., 2016), partly because the former was not measured in syn-rift formation. The boundary of D3 and D4 phases can correspond to the onset of rifting probably around 18.2 Ma (Fig. 7).

In any case, the D4 early rifting phase predated the first R1 CCW rotation (Márton and Fodor, 1995). The oldest pyroclastic levels of the Pannonian Basin registered palaeomagnetically this R1 rotation; the new age data of different eruptions are between 17.3 and 17.1 Ma (Tihamér Formation, Lukács et al., 2022; and Eger-Ipolytarnóc Member, Karátson et al., 2022; Brlek et al., 2023). This suggests a pre–17.1 Ma for the observed D4 phase of N-S extension (Fig. 7).

After the R1 rotation, the F1 fracture system was followed by a NE–SW extensional phase (F2a stress state) which is marked by NW–striking normal faults. The extensional stress regime F2a was measured in one syn-rift (Ps–15) and few pre-rift sites of the study area (Fig. 6., CSER22–01, −16, −23–27) and is very frequent in the closer vicinity (Cs–07, −08, −11, −14) and in the wider surroundings (Fig. 7, Beke, 2016; Beke et al., 2019). In the northern Pannonian Basin, NE–SW extension resulted in a dense network of NW–striking normal faults; the related tilted blocks and half-grabens are ubiquitous character of the entire northern basin half (Csontos, 1995; Petrik et al., 2016; Ruszkiczay-Rüdiger et al., 2009; Tari et al., 1992, Fig. A3).

The F2b stress state is marked by a strike-slip regime of NW–SE compression and NE–SW extension. The important fractures are E–W striking dextral and NNW–SSE striking sinistral faults (CsSER22–07, Cs–06, −08 sites, Fig. 6). The relative chronology of the F2b and F1 stress regimes is relatively clear, because F2b E–W striking dextral faults reactivated earlier normal faults or joints of the F1 fracture set, particularly in sites CSER22–07 and Cs–08 (Fig. 6). This strike-slip stress regime is not widespread but occurs locally in the Pannonian Basin (Bada et al., 1996; Fodor et al., 1999; Fodor, 2011; Oláh et al., 2014). The NE–SW extensional stress state F2a share the same direction of minimal stress axes; thus, we consider that the two fracturing events (F2a and F2b) belonging to the same deformation phase which can be correlated with the D5 regional phase (Fig. 7), as suggested by earlier studies (Figs. 7, and A4; Beke et al., 2019; Benkovics, 1991; Fodor et al., 1999; Vass et al., 1993). This regional D5 phase had to follow the first rotation event because it affected the already rotated magmatic rocks. The time span of rotation is not defined sharply, and the gradual rotation induced equally smooth change in the stress axes. Thus, D4 and D5 phases (F1 and F2 local fracture system) could be transitional in their structural directions (Fig. 7). However, this phase certainly followed the Bogács pyroclastic level and may have started around 16.8 Ma. The F2 fracture sets clearly deform the Visegrád Complex (15.4–15.3 Ma, Beke et al., n.d.), and part of the Eastern Cserhát Volcanic Complex (Fig. A3). The upper boundary of F2 fracture seems to be younger than the 14.9 Ma old Tar Dacite Lapilli Tuff Formation ("Jató Mb." by Biró et al., 2020), because the F2 fracture system was also observed in the type locality Tar. The upper time constraint for D5 phase is given by the second rotation, which can be roughly bracketed between ~14.8 and ~ 14 Ma (Fig. 7).

According to our new geochronological data, the dyke emplacement (F3 fracturing event) with E–W to NW–SE strike has taken place around 15.4 Ma. The NNW–SSE striking dykes are younger having an age of 14.66 ± 0.58 Ma. This means that the dykes developed in two cycles. Regarding their age, and the existing but far less dominant strike (NW–SE) of the older dykes, they formed within the D5 deformation phase during the earliest Middle Miocene.

Dyke emplacement tends to be perpendicular to the extension (Guðmundsson, 1995; Hou et al., 2010; Pollard, 1987). This would mean a N-S extension for the E–W trending dykes, like F1 fracture set, or the D4 phase. However, since dykes are younger than D4 phase by a minimum of 1.4 Ma, they could hardly have formed in D4 phase. Thus, we infer the E-W-striking dykes are marked by a specific stress field not corresponding the regional stress field. This may indicate that the dykes formed under the presence of local stress field at volcanic centres feeding the dykes, or that the dykes propagated along pre-existing zones of weaknesses on older normal faults formed in the preceding deformation phase. Formation of a dyke with segments of different strike, caused by interaction of the effects of local stress field caused by topography of a volcanic centre, and stress to due plate movements, has for example been observed in the Bárðarbunga volcanic system, Iceland in 2014 (Sigmundsson et al., 2015). The interpretation of joints perpendicular to E–W-striking dykes is not easy in the frame of regional stress field (Fig. 6). However, dyke-perpendicular cooling joints were observed by Townsend et al. (2015), and by Shukla et al. (2022). Townsend et al. (2015) suggested that these joints formed because of dyke intrusion combined with thermal expansion of pore fluids.

We separated a transitional fracture set F4 which is marked by minimal stress axis directions between ENE–WSW and E–W (Figs. 6, and 7) (Juhász et al., 2023). This fracture set post-dated the southern dyke emplacement (Csörög and János Hill dykes) because the cooled dyke rock was deformed by F4 fracture system. Map-scale faults also displace the entire stratigraphic column up to the Hasznos Volcanoclastics near sites CSER22–07 and Ps–15 (Fig. 4) and bound the Galga Graben just east of those sites (Fig. A3). Other map-scale examples include the tilted blocks of Gödöllő (Fig. A3). Looking at the spread of extensional directions, we correlate the F4 fracture set to the time span of the second R2 rotation.

While there are few structural data from well-dated volcanic sites, we suggest the transition from F2 to F5 fracture system (or D5 to D6 regional phase) between 14.8 and ~ 14 Ma (Fig. 7). Paleomagnetic data do not permit a sharp definition of the timing of this rotation event, as few sites show the rotation, and others are not from the same pyroclastic horizons (14.9 Ma Tar, and 14.4 Ma Harsány, Zelenka et al., 2004, Márton et al., 2007b; Lukács et al., 2018). However, late Badenian rocks

younger than 13.8 Ma never exhibit F4 fractures, but only the F5 set. Thus, a broader time span of ~14.8 to ~14 Ma can be suggested for R2 rotation and F4 fractures. The Kisgéc dyke fits to the gradual transition of the stress field. Assuming dyke–perpendicular extension, this dyke swarm can be controlled by the F4 fracture set. The stress regime of the F4 fractures and the northern Kisgéc dykes can be classified into the transition of D5 and D6 phases (Fig. 7). Similar stress field was reported by Márton and Fodor (1995), and Vass et al. (1993) from the surrounding regions in south Slovakia, and north Hungary (Fig. A1). Vojtko et al. (2019) also observed F4 fracture set marked by a strike-slip regime (Fig. A1). Their suggested timing is somewhat younger, from ca. 14 to 11.6 My, than our time constraints of 14.8–14 Ma, but this may not represent a large contradiction (Fig. A1).

The two youngest fracture sets F5 and F6, an E–W and SE–NW extension, occurred after the rotation, and these fractures deformed the late Badenian and younger rocks. Several major NNE–striking normal faults and related tilted blocks mark the half-graben system of the Zagyva basin, from the Eastern Cserhát Volcanic Complex down to the Buda Hills (Benkovics, 1991; Fodor et al., 1999; Soós, 2017, Fig. A3), reported in fault-slip analyses (Figs. 7, and A1) (Beke et al., 2019; Vass et al., 1993; Vojtko et al., 2019). The question if the F5 and F6 fracture sets represent two separate regional phases, or just local variations in the extensional direction, this question needs further studies. However, all these fractures post-date R2 rotation, and also the younger dyke generation of the northern Cserhát Hills.

5.2.2. Magma migration

The structural data show that the study area was strongly fractured due to the Miocene rifting, and these faults may have interacted with some of the dyke segments. A lithological discontinuity had eventually also a strong influence on the dyke emplacement. Several studies have showed that the presence of contrasting mechanical properties, e. g., a relatively weak layer above a more competent layer, has strong influence on dyke propagation. In general, lateral emplacement along a lithology change boundary may be favoured over vertical propagation (Bazargan and Guðmundsson, 2019; Drymoni et al., 2020; Pinel and Jaupart, 2004; Walker et al., 2017). Additionally, numerical models of dyke formation in a crust with soft layers and weak contacts show concentration of stress change in zones near a dyke but also where there are strong gradients in crustal strength (Guðmundsson and Loetveit, 2005). Basin infilling sedimentary rocks consisting of poorly lithified sandstone or siltstone ("schlier" in the local terminology, see Introduction), near surface at the time of formation of the dykes, may have acted as a weak layer. We suggest that arrest or lateral propagation of dykes in our study area may have been influenced by lithological inhomogeneity in the crust at the time of emplacement. This may explain why several dykes can be followed for up to 23 km in the Cserhát Hills while they do not climb considerably upward or downward in the stratigraphy (see the Hegyes dykes, Figs. 3 and A3). It is also possible that pre-dyking extensional tectonic stress field in the area induced by plate tectonics, combined with weak material near surface of lower density than the magma facilitated long-distance lateral magma transport; (Sigmundsson et al., 2022).

In the stratigraphy of the study area, several formations have fine-grained composition: the latest Oligocene to lowermost Miocene Szécsény, the lower part of the Lower Miocene Salgótarján and the whole Garáb Formations. These formations were reached by the Hegyes, Bercel, and Kisgéc dykes. Therefore, based on Guðmundsson and Loetveit (2005), we propose that, when the ascending magma encountered less rigid formation with sand composition, fissure volcanoes and volcanic cones may have formed (upper part of the Salgótarján Formation, and Fót Formation). For example, this may have occurred in the southern area, where the magma reached the Fót Formation very close to the surface and resulted in eruptions (fissure volcanoes and/or surficial lava flows). Along the volcanic centres in the central Cserhát Hills (Szanda, Bercel, Bér, Fig. A3) the situation could be similar, where the ascending magma has reached the sandy or carbonate part of the Lower Miocene host rocks, which belong to the lowermost part of the *syn*-rift sequence.

5.2.3. Interaction of dyke and faults – Stress field inhomogeneity

Dykes in our study area were emplaced into fractures formed during D3 – D4 phases (Fig. 7). The last and intensive D4 phase (marked by ~N–S extension), acted ca. 1.5 Ma before emplacement of most of the dykes (Fig. 8a).

Our fault-slip data and field observations suggest two possible scenarios for the stress field that operated during dyke emplacement. In one case, the dyke segments mostly propagated along dextral strike-slip faults (Figs. 8d, and A2), although the systematic en echelon geometry, typical for strike-slip secondary faults, are only locally present (Fig. 4). In site Ps-2 the dextral faults observed in the host rock (Fig. 6), are just few tens of centimetres distance from the dyke wall. In addition, large, km-scale dextral faults were documented both west and east of the outcropping dykes (Figs. 2c, and 3). One of the largest displacements occurs near site Cs–08 where the base–syn-rift horizon shows 2–2.7 km dextral offset (Fig. 1b and A3). Another important offset of the base–syn-rift horizon is found in the eastern continuation of the Bercel dyke; this fault bound a Paleogene horst on the south, and continuous in the Zagyva graben as a transfer fault between two tilted block domains (Figs. 1b, 2c, and A3, Soós, 2017). In a study of the Neuquén back-arc Basin, Spacapan et al. (2016) suggested that the dyke did not propagate perpendicular to the σ_3 axis, but along a pre-existing strike-slip fault, having a similar scenario as in the case of Cserhát Hills. A possible third case is the connection of faults of the Visegrád Complex and the Csörög and János Hill dykes of the southern Cserhát Hills (Figs. 1b, and A3). E–W striking dextral faults were mapped and kinematically characterised in the Visegrád Mts. (e.g., Dömös-Tahi Fault, Balla and Korpás, 1980; Beke et al., n.d.; Bence et al., 1991), imaged below the Danube by seismic reflection data (Oláh et al., 2014), and can be projected toward the dykes. The age of the Visegrád Complex (15.30 ± 0.24 to 15.40 ± 0.25 Ma, Beke et al. submitted) is very close to the age of the Cserhát dykes (14.5 ± 0.21 to 15.3 ± 0.22 Ma), making reasonable the proposed interaction between faults and dyke segments. Contemporaneous dyke intrusion and strike-slip faulting has also been documented in Iceland in recent volcano-tectonic systems, e.g., at the Fagradalsfjall volcanic system in 2021 (Sigmundsson et al., 2022), as well as in the Barðarbunga volcanic system in 2014, where in both cases strike-slip faulting occurred near dyke propagation (Plateaux et al., 2014; Ágústsdóttir et al., 2016). In addition to previous fault-slip studies, we suggest that dyke emplacement was at least partly coeval with this dextral faulting (Figs. 8d, and A1).

Coeval dyke propagation, magma overpressure and faulting can alter the surrounding stress field (Guðmundsson et al., 2009). In such situations, an increase of the maximal horizontal stress axes may create a strike-slip regime that temporally and locally may overwrite the otherwise dominant extensional regime. This may have occurred in our study area (Figs. 8d, and A2). In an extensional and strike-slip context such as Iceland, permutations of stress axes and local strike deflections of stress may be quite common and linked both to the tectonic process and magmatic activity. Stress permutations may occur on a long time (a few Myr) but also quasi instantaneously as demonstrated by analysis of focal mechanisms of earthquakes as well (e.g., Bergerat and Angelier, 2008). Such stress axes permutation is frequent in fault-slip analyses and may reflect e.g., spatial change in rock rheology connected to density of fractures, lithological changes in weak zones (Angelier and Bergerat, 1983; Hu and Angelier, 2004) or, near the dykes, alteration of host rock stress by magmatic fluids (Ágústsdóttir et al., 2016). Thus, despite the difference in the general tectonic context; rift and oceanic transforms observed in Iceland, and back-arc basin in the Pannonian Basin, we note similarities in the fault-dyke interaction. In the Pannonian Basin, this stress axes permutation and alteration can explain the occurrence of, albeit limited, strike-slip faulting within the regionally extensional stress

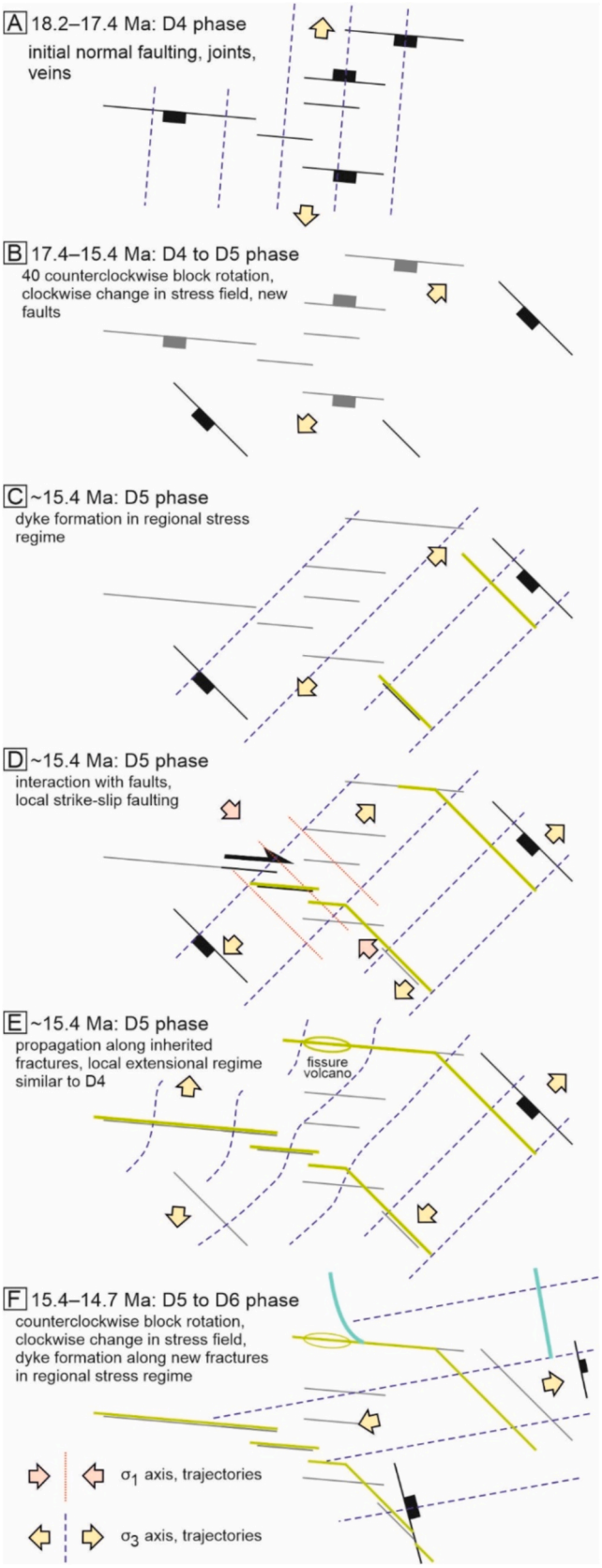

Fig. 8. Simplified summary of structural evolution. Note how the dykes interacted with preexisting and active fractures and how dyke emplacement modified the regional stress field. See a three-dimension version of the model of dykes, fractures and stress trajectories in Fig. A2.

field even if the direction of the extensional stress axis did not change (Figs. 6 and 8).

As we analysed earlier, the N-S extension corresponds to D4 regional deformation phase (Fig. 8a). Thus, the interaction of dyke emplacement and pre-existing fractures locally changed the stress axes to a direction which was already occupied during the previous deformation phase, just prior to dyke emplacement. This could result in curved stress trajectories starting from "average" NE–SW extension to N-S extension near the dyke tip (Figs. 8e and A2).

After the first dyke emplacement, the area suffered counter-clockwise rotation, which is reflected in the fault-slip data as a clock-wise change in σ_{Hmax} between D5 and D6 regional phases (F2 to F5 fracture sets, Fig. 6). During this rotation and stress field change, the younger Kisgéc dyke formed, presumably perpendicular to the regional extensional direction (Fig. 8f). Associated F5 fractures deformed the older dykes, and map-scale normal faults cut across the Csörög and János Hill dykes (Figs. 4, and 8f). The R2 rotation is younger than the older dyke set of 15.4 Ma but was ongoing during the younger dyke emplacement. If we combine fault-slip data from the Tar Formation the onset of this R2 rotation is between 14.9 and 14.7 Ma. This onset seems to be younger than in other studies which placed the entire rotation before 15 Ma (Lukács et al., 2015; Márton and Fodor, 1995). Our study shows that inferring regional stress axis from strike of dykes may have shortcomings, as there are many processes that influence the orientation of dike planes. Our observations can be used as constraints in future modelling studies of dyke propagation paths, improving understanding of how dykes are affected by crustal heterogeneities and pre-existing fractures (e.g., Drymoni et al., 2021; Greiner et al., 2023; and Maccaferri et al., 2016).

5.2.4. *The effect of the dykes in later structural evolution*

The dykes, representing strong rheological heterogeneity influenced the latest evolution of fracturing. This can be seen in the structure of the Zagyva graben, where a regional transfer fault of the D6 phase between two extensional tilted block domains (Soós, 2017) follows the pre-existing Bercel dyke (east of the locations CSER22–08 and CSER22–09). This dyke belonging to the Hasznos Volcaniclastics may have been originally emplaced along a pre–existing D4 normal or coeval D5 dextral fault, that changed to sinistral transfer faults during later graben formation (D6 phase) (Fig. A3). This suggests that the partitioning of tilted block domains was influenced by the presence (and orientation) of the D4 phase normal faults and D5 phase dykes. The postulated "cross-faults" of Noszky (1940) can also be explained by the presence of dykes. Namely, these cross faults may be related to stepovers of dyke segments or could follow cooling joint set within the dyke material (See Fig. A2).

6. Conclusions

This study describes the interaction of volcanism, dyking, pre-existing and coeval faulting in a continuously changing regional stress regime in the Cserhát Hills, thereby providing new insights into dyking events and stress changes in the northern Pannonian Basin.

The combined field and geochronological data help to clarify the geological process involved and timing of deformation events. Six separated main fracturing events, named by F1 to F6, may correlate to previously identified regional deformation phases. The geochronological data support that the dykes were emplaced in two different eruptive cycles, the NW–SE to E–W striking (older) dykes with ~15.4 Ma age, and the NNW–SSE striking (younger) dykes with an age of ~14.7 Ma. Along the ~E – W oriented dyke segments the dyke may have propagated into coeval strike-slip faults and followed their strike, thus induced the permutation of the maximal and intermediate stress axes. On the other hand, interaction of dyke emplacement may have reactivated earlier normal faults and resulted in local counter-clockwise rotation of minimal stress axis, as it can be seen at the inclined dyke of site CSER22–21.

Therefore, it may not be possible to infer the regional stress regime based only on the dyke orientation, because of its heterogeneity induced by the dyking event itself.

Furthermore, extensive horizontal-dyke emplacement may be facilitated by lithological difference between the pre-rift sandstone-siltstone formations and the overlying basal, fine-grained early *syn*-rift formations. New observation and previously collected dataset from the field, as well as the field observations show that dyke emplacement does not always follow the regional stress regime. Rather, reactivated faults formed earlier, with variable kinematics, may have influenced the dyke emplacement.

CRediT authorship contribution statement

Dorina Juhász: Writing – review & editing, Writing – original draft, Conceptualization. **Chiara Lanzi:** Writing – review & editing, Methodology. **Zsolt Benkó:** Writing – review & editing, Methodology. **Freysteinn Sigmundsson:** Writing – review & editing, Methodology. **Barbara Beke:** Writing – review & editing. **Françoise Bergerat:** Writing – review & editing. **László Fodor:** Writing – review & editing, Supervision, Funding acquisition, Conceptualization.

Declaration of competing interest

The authors declare that they have no known competing financial interests or personal relationships that could have appeared to influence the work reported in this paper.

Acknowledgement

We acknowledge extensive suggestions and comments from two reviewers and the editor, that helped us to greatly improve the manuscript. The study was supported by grant 134873 of the National Research, Development and Innovation Office of Hungary led by László Fodor and by grant 139275 of the National Research, Development and Innovation Office of Hungary led by Barbara Beke.

Appendix A. Supplementary data

Supplementary data to this article can be found online at https://doi.org/10.1016/j.tecto.2025.230722.

Data availability

Data will be made available on request.

References

Ágústsdóttir, T., Woods, J., Greenfield, T., Green, R.G., White, R.S., Winder, T., Brandsdóttir, B., Steinthórsson, S., Soosalu, H., 2016. Strike-slip faulting during the 2014 Bárðarbunga–Holuhraun dike intrusion, central Iceland. Geophys. Res. Lett. 43 (4), 1495–1503. https://doi.org/10.1002/2015GL067423.

Anderson, E.M., 1937. IX.—the Dynamics of the Formation of Cone-sheets, Ring-dykes, and Caldron-Subsidences. Proc. R. Soci. Edinburgh 56, 128–157. https://doi.org/10.1017/S0370164600014954.

Anderson, E.M., 1951. The Dynamics of Faulting and Dyke Formation with Applications to Britain, Second ed. Oliver and Boyd, Edinburgh, UK.

Angelier, J., 1984. Tectonic analysis of fault slip data sets. J. Geophys. Res. Solid Earth 89 (B7), 5835–5848. https://doi.org/10.1029/JB089iB07p05835.

Angelier, J., Bergerat, F., 1983. Systèmes de contrainte et extension intracontinentale [Stress systems and continental extension]. In: Bulletin des Centres de Recherches Exploration – Production Elf-Aquitaine, 7, pp. 137–147.

Angelier, J., Manoussis, S., 1980. Classification automatique et distinction des phases superposée en tectonique de failles. Comptes Rendues de l'Académie des Sciences Paris 290, série D, pp. 651–654.

Bada, G., Fodor, L., Székely, B., Timár, G., 1996. Tertiary brittle faulting and stress field evolution in the Gerecse Mountains, northern Hungary. Tectonophysics 255 (3–4), 269–289. https://doi.org/10.1016/0040-1951(95)00141-7.

Báldi, T., 1986. Mid-Tertiary Stratigraphy and Paleogeographic Evolution of Hungary. Akadémiai Kiadó, Budapest, Hungary.

Balla, Z., Korpás, L., 1980. Methodological questions of the mapping of volcanics in the Dunazug Mountains, N Hungary. Annual Report, Geological Institute of Hungary from 1978, 233–238.

Báldi, T., Báldi-Beke, M., 1985. The evolution of the Hungarian Paleogene basins. Acta Geol. Hung. 28 (1–2), 5–28.

Balla, Z., 1989. Reevaluation of the Diósjenő dislocation zone. Annual Report, Eötvös Loránd Geophysical Institute from 1987, pp. 45–57.

Balogh, K., 1984. Introduction of the K/Ar Method and First Results. Unpublished candidate theses of the Hungarian Academy of Sciences (in Hungarian).

Bazargan, M., Guðmundsson, A., 2019. Dike-induced stresses and displacements in layer volcanic zones. J. Volcanol. Geotherm. Res. 384, 189–205. https://doi.org/10.1016/j.jvolgeores.2019.07.010.

Beke, B., 2016. Role of Deformation Bands in Structural Evolution of Cenozoic Porous Sediments in NE Hungary (PhD Thesis).. MTA–ELTE Geological, Geophysical and Space Science Research Group, Eötvös University, Budapest.

Beke, B., Fialowski, M., Müller, T., Schubert, F., Lukács, R., Guillong, M., Harangi, Sz., Fodor, L. (in revision). Structurally controlled silica precipitation within multi-stage fault damage zones during the rifting of the Pannonian Basin. Basin Research.

Beke, B., Fodor, L., Millar, L., Petrik, A., 2019. Deformation band formation as a function of progressive burial: Depth calibration and mechanism change in the Pannonian Basin (Hungary). Mar. Pet. Geol. 105, 1–16. https://doi.org/10.1016/j.marpetgeo.2019.04.006.

Bence, G., Császár, G., Darida-Tichy, M., Dudko, A., Gálos, M., Gangl, G., Kertész, P., Korpás, L., Zier, C., 1991. Geologische und ingenieurgeologische Beschreibung der Donaustufe Nagymaros. In: Lobitzer, H., Császár, G. (Eds.), Jubiläumsschrift 20 Jahre geologische Zusammenarbeit Österreich-Ungarn 1, pp. 385–400.

Benkő, K., Fodor, L., 2002. Structural geology near Csővár, Hungary. Földtani Közlöny 132, 223–246.

Benkovics, L., 1991. A Zagyva–árokban végzett mikrotektonikai vizsgálatok és szeizmikus szelvényekkel való kapcsolata. MSc thesis. Eötvös Loránd University, Budapest (in Hungarian).

Bergerat, F., Angelier, J., 2008. Immature and mature transform zones near a hot spot: the South Iceland Seismic Zone and the Tjörnes Fracture Zone (Iceland). Tectonophysics 447, 142–154. https://doi.org/10.1016/j.tecto.2006.05.046.

Bergerat, F., Geyssant, J., Lepvrier, C., 1984. Neotectonic outline of the Intra–Carpathian basins in Hungary. Acta Geol. Hung. 27, 237–251.

Biró, T., Hencz, M., Németh, K., Karátson, D., Márton, E., Szakács, A., Bradák, B., Szalai, Z., Pécskay, Z., Kovács, I., 2020. A Miocene Phreatoplinian eruption in the North–Eastern Pannonian Basin, Hungary: The Jató Member. J. Volcanol. Geotherm. Res. 401, 106973. https://doi.org/10.1016/j.jvolgeores.2020.106973.

Brlek, M., Tapster, S.R., Schindlbeck–Belo, J., Gaynor, S.P., Kutterolf, S., Hauff, F., Georgiev, S.V., Trinajstić, N., Šuica, S., Brčić, V., Wang, K.-L., Lee, Y.-H., Beier, C., Abersteiner, A.B., Mišur, I., Peytcheva, I., Kukoč, D., Németh, B., Trajanova, M., Balen, D., Guillong, M., Szymanowski, D., Lukács, R., 2023. Tracing widespread Early Miocene ignimbrite eruptions and petrogenesis at the onset of the Carpathian–Pannonian Region silicic volcanism. Gondwana Res. 113, 40–60. doi: https://doi.org/10.1016/j.gr.2022.12.015.

Budai, T., Chikán, G., Csillag, G., Fodor, L., Koloszár, L., Magyari, Á., Németh, K., Selmeczi, I., 2005. Magyarázó Püspökszilágy környékének előzetes földtani térképéhez, M=1:10 000. Unpublished report Geological Institute of Hungary. Budapest and Mecsekérc Ltd., Pécs, Hungary, 123 p.

Cassignol, C., Gillot, P.-Y., 1982. Range and effectiveness of unspiked potassium–argon dating: experimental groundwork and applications. In: Odin, G.S. (Ed.), Numerical Dating in Stratigraphy. John Wiley & Sons, pp. 159–179, 1982.

Csontos, L., 1995. Tertiary tectonic evolution of the Intra-Carpathian area: a review. Acta Vulcanol. 7, 1–13.

Csontos, L., Nagymarosy, A., 1998. The Mid-Hungarian line: a zone of repeated tectonic inversions. Tectonophysics 297 (1–4), 51–71. https://doi.org/10.1016/S0040-1951(98)00163-2.

Csontos, L., Tari, G., Bergerat, F., Fodor, L., 1991. Evolution of the stress fields in the Carpatho–Pannonian area during the Neogene. Tectonophysics 199, 73–91. https://doi.org/10.1016/0040-1951(91)90119-D.

Dahm, T., 2000. Numerical simulations of the emplacement path and the arrest of fluid–filled fractures in the Earth. Geophys. J. Int. 141 (3), 623–638. https://doi.org/10.1046/j.1365-246x.2000.00102.x.

Daniels, K.A., Menand, T., 2015. An experimental investigation of dyke injection under regional extensional stress. J. Geophys. Res. Solid Earth 120 (3), 2014–2035. https://doi.org/10.1002/2014JB011627.

Delaney, P.T., Pollard, D.D., Ziony, J.I., McKee, E.H., 1986. Field relations between dikes and joints: Emplacement processes and palaeostress analysis. J. Geophys. Res. Solid Earth 91, 4920–4938. https://doi.org/10.1029/JB091iB05p04920.

Drymoni, K., Browning, J., Guðmundsson, A., 2020. Dyke–arrest scenarios in extensional regimes: Insights from field observations and numerical models, Santorini, Greece. J. Volcanol. Geotherm. Res. 396, 106854. https://doi.org/10.1016/j.jvolgeores.2020.106854.

Drymoni, K., Browning, J., Guðmundsson, A., 2021. Volcanotectonic interactions between inclined sheets, dykes, and faults at the Santorini Volcano, Greece. J. Volcanol. Geotherm. Res. 416, 107294. https://doi.org/10.1016/j.jvolgeores.2021.107294.

Dunkl, I., Frisch, W., 2002. Thermochronologic constraints on the late Cenozoic exhumation along the Alpine and West Carpathian margins of the Pannonian basin. In: Cloetingh, S.A.P.L., Horváth, F., Bada, G., Lankreier, A.C. (Eds.), Neotectonics and Surface Processes: The Pannonian Basin and Alpine/Carpathian System, EGU Stephan Mueller Special Publication Series, vol. 3, pp. 120–134.

Fodor, L., 2011. Mezozoos–kainozoos feszültségmezők és törésrendszerek a Pannon-medence ÉNy-i részén–módszertan és szerkezeti elemzés Manuscript Hungarian

Academy of Sciences (in Hungarian). https://real-d.mtak.hu/343/4/dc_63_10_doktori_mu.pdf.
Fodor, L., Magyari, A., Kázmér, M., Fogarasi, A., 1992. Gravity-flow dominated sedimentation on the Buda paleoslope (Hungary): Record of Late Eocene continental escape of the Bakony Unit. Geol. Rundsch. 81, 695–716.
Fodor, L., Csontos, L., Bada, G., Györfi, I., Benkovics, L., 1999. Tertiary tectonic evolution of the Pannonian basin system and neighboring orogens: a new synthesis of palaeostress data, in: Durand, B., Jolivet, L., Horváth, F., Séranne, M., (Eds), The Mediterranean Basins: Tertiary extension within the Alpine Orogen. Geol. Soc. Lond. Spec. Publ. 156, 295–334. https://doi.org/10.1144/GSL.SP.1999.156.01.15.
Fusán, O., Zoubek, V., 1964. Geological map of Slovakia, 1:200.000, Zvolen M–34–XXXII. Dionyz Stúr Geological Insitute of Slovak Republic.
Gál, P., Lukács, R., 2024. Mátra Andezite Complex. In: Babinszki, E., Piros, O., Csillag, G., Fodor, L., Gyalog, L., Zs, Kercsmár, Gy, Less, Lukács, R., Sebe, K., Selmeczi, I., Szepesi, J., Sztanó, O. (Eds.), Lithostratigraphic units of Hungary II. Cenozoic formations. SZTFH and Hungarian Academy of Sciences, Stratigraphic Sub–Committee, Budapest, Hungary, pp. 81–83.
Gillot, P.-Y., Cornette, Y., 1986. The Cassignol technique for potassium–argon dating, precision and accuracy: examples from late Pleistocene to recent volcanics from southern Italy. Chem. Geol. Isotope Geosci. Section 86, 205–222. https://doi.org/10.1016/0168-9622(86)90072-2.
Gillot, P.-Y., Cornette, Y., Max, N., Floris, B., 1992. Two reference materials, trachyte MDO-G and ISH-G for argon dating (K/Ar and $^{40}Ar/^{39}Ar$) of Pleistocene and Holocene rocks. Geostand. Newslett. 15, 55–60. https://doi.org/10.1111/j.1751-908X.1992.tb00487.x.
Greiner, S.H.M., Burchardt, S., Sigmundsson, F., Óskarsson, B.V., Galland, O., Geirsson, H., Rhodes, E., 2023. Interaction between propagating basaltic dikes and pre-existing fractures: a case study in hyaloclastite from Dyrfjöll, Iceland. J. Volcanol. Geotherm. Res. 442, 107891. https://doi.org/10.1016/j.jvolgeores.2023.107891.
Guðmundsson, Á., 1984. Formation of dykes, feeder-dykes, and the intrusion of dykes from magma Chambers. Bull. Volcanol. 47, 537–550. https://doi.org/10.1007/BF01961225.
Guðmundsson, Á., 1995. The geometry and growth of dykes. Phys. Chem. Dykes 23–34.
Guðmundsson, Á., 2002. Emplacement and arrest of sheets and dykes in central volcanoes. J. Volcanol. Geotherm. Res. 116, 279–298. https://doi.org/10.1016/S0377–0273(02)00226–3.
Guðmundsson, Á., 2006. How local stresses control magma-chamber ruptures, dyke injections, and eruptions in composite volcanoes. Earth Sci. Rev. 79, 1–31. https://doi.org/10.1016/j.earscirev.2006.06.006.
Guðmundsson, Á., Brenner, S.L., 2004. Local stresses, dyke arrest and surface deformation in volcanic edifices and rift zones. Ann. Geophys. 47, 1433–1454. https://doi.org/10.4401/ag–3352.
Guðmundsson, Á., Loetveit, I.F., 2005. Dyke emplacement in a layer and faulted rift zone. J. Volcanol. Geotherm. Res. 144, 311–327. https://doi.org/10.1016/j.jvolgeores.2004.11.027.
Guðmundsson, A., Friese, N., Andrew, R., Philipp, S.L., Ertl, G., Letourneur, L., 2009. Effects of Dyke Emplacement and Plate Pull on Mechanical Interaction between Volcanic Systems and Central Volcanoes in Iceland. In: Studies in Volcanology: The Legacy of George Walker, T. Thordarson, S. Self, G. Larsen, S. K. Rowland, Á. Höskuldsson. https://doi.org/10.1144/IAVCEl002.17.
Gyalog, L., Síkhegyi, F. (Eds.), 2005. Magyarország Földtani Térképe (Geological map of Hungary), M=1:100000. Geological Institute of Hungary, Budapest.
Hámor, G., 1985. Geology of the Nógrád–Cserhát area. Geologica Hungarica, ser. Geol. 22,, 234 p.
Harangi, Sz, 2001. Neogene to Quaternary volcanism of the Carpathian–Pannonian Region—a review. Acta Geol. Hung. 44, 223–258.
Harangi, Sz, Lenkey, L., 2007. Genesis of the Neogene to Quaternary volcanism in the Carpathian–Pannonian region: Role of subduction, extension, and mantle plume. Geol. Soc. Am. Spec. Pap. 418, 67. https://doi.org/10.1130/2007.2418(04).
Harangi, Sz, Seghedi, I., Lukács, R., 2024. The Neogene–Quaternary volcanism of the Carpathian–Pannonian region: from initial plate tectonic models to quantitative petrogenetic explanations. In: Tari, G., Kitchka, A., Krézsek, Cs, Lučić, D., Markič, M., Radivojević, D., Sachsenhofer, R.F., Šujan, M. (Eds.), The Miocene Extensional Pannonian Superbasin, Volume 1: Regional Geology. Geological Society, London. https://doi.org/10.1144/SP554-2024-66. Special Publications 554.
Heimisson, E.R., Hooper, A., Sigmundsson, F., 2015. Forecasting the path of a laterally propagating dike. J. Geophys. Res. Solid Earth 120, 8774–8792. https://doi.org/10.1002/2015JB012402.
Hess, J.C., Lippolt, H.J., 1994. Compilation of K–Ar measurements on HD–B1 standard biotite: 1994 status report. In: Odin, G.S. (Ed.), Calibration of the Phanerozoic Time Scale, IGCP Proj. 196. IUGS 29. Subcommision on Geochronology, International Geological Correlation Programme, Paris, pp. 19–23.
Hetényi, G., Taisne, B., Garel, F., Médard, É., Bosshard, S., Mattsson, H.B., 2012. Scales of columnar jointing in igneous rocks: field measurements and controlling factors. Bull. Volcanol. 74, 457–482. https://doi.org/10.1007/s00445-011-0534-4.
Horváth, F., Musitz, B., Balázs, A., Végh, A., Uhrin, A., Nádor, A., Koroknai, B., Pap, N., Tóth, T., Wórum, G., 2015. Evolution of the Pannonian basin and its geothermal resources. Geothermics 53, 328–352. https://doi.org/10.1016/j.geothermics.2014.07.009.
Hou, G., Kusky, T.M., Wang, C., Wang, Y., 2010. Mechanics of the giant radiating Mackenzie dyke swarm: a paleostress field modeling. J. Geophys. Res. Solid Earth 115. https://doi.org/10.1029/2007JB005475 no. B2.
Hu, J.C., Angelier, J., 2004. Stress permutations: Three–dimensional distinct element analysis accounts for a common phenomenon in brittle tectonics. J. Geophys. Res. Solid Earth 109, B09403. https://doi.org/10.1029/2003JB002616.
Jäger, E., Ji, C.W., Hurford, J.A., Xin, L.R., Hunziker, J.C., Ming, L.D., 1985. BB-6: a quaternary age standard for K/Ar dating. In: Chemical Geology: Isotope Geoscience Section 52/3–4, pp. 275–279. https://doi.org/10.1016/0168-9622(85)90039-9.
Juhász, D., Lanzi, C., Váradi, K., Szijártó, M., Fodor, L., Sigmundsson, F., 2023. Numerical modeling of Miocene dyke opening in the Cserhát Hills, Hungary, EGU General Assembly 2023, Vienna, Austria, 24–28 Apr 2023, EGU23–458, p. 2023. https://doi.org/10.5194/egusphere–egu23–458.
Karátson, D., 2007. A Börzsönytől a Hargitáig. Typotex Press, Budapest, 463 pp.
Karátson, D., Biró, T., Portnyagin, M., Kiss, B., Paquette, J.-L., Cseri, Z., Hencz, M., Németh, K., Lahitte, P., Márton, E., Kordos, L., Józsa, S., Hably, L., Müller, S., Szarvas, I., 2022. Large–magnitude (VEI ≥ 7) 'wet' explosive silicic eruption preserved a Lower Miocene habitat at the Ipolytarnóc Fossil Site, North Hungary. Scientific Rep. 12 (1), 9743. https://doi.org/10.1038/s41598–022–13586–3.
Kováč, M., Hudáčková, N., Halásová, E., Kováčová, M., Holcová, K., Oszczypko-Clowes, M., Báldi, K., Less, G., Nagymarosy, A., Ruman, A., Klučiar, T., 2017. The Central Paratethys palaeoceanography: a water circulation model based on microfossil proxies, climate, and changes of depositional environment. Acta Geologica Slovaca 9 (2).
Lahitte, P., Dibacto, S., Karátson, D., Gertisser, R., Vreres, D., 2019. Eruptive history of the late Quaternary Ciomadul (Csomád) volcano, East Carpathians, part I: timing of lava dome activity. Bull. Volcanol. 81 (4), 27. https://doi.org/10.1007/s00445–019–1286–9.
Lukács, R., Sz, Harangi, Bachmann, O., Guillong, M., Danišík, M., Buret, Y., von Quadt, A., Dunkl, I., Fodor, L., Sliwinski, J., Soós, I., Szepesi, J., 2015. Zircon geochronology and geochemistry to constrain the youngest eruption events and magma evolution of the Mid-Miocene ignimbrite flare-up in the Pannonian basin, eastern–Central Europe. Contrib. Mineral. Petrol. 170 (52). https://doi.org/10.1007/s00410-015-1206-8, 26pp.
Lukács, R., Harangi, S., Guillong, M., Bachmann, O., Fodor, L., Buret, Y., Dunkl, I., Sliwinski, J., von Quadt, A., Peytcheva, I., Zimmerer, M., 2018. Early to Mid-Miocene syn-extensional massive silicic volcanism in the Pannonian Basin (East–Central Europe): Eruption chronology, correlation potential and geodynamic implications. Earth Sci. Rev. 179, 1–19. https://doi.org/10.1016/j.earscirev.2018.02.005.
Lukács, R., Guillong, M., Bachmann, O., Fodor, L., Harangi, Sz, 2021. Tephrostratigraphy and magma evolution based on combined zircon trace element and U–Pb age data: Fingerprinting Miocene silicic pyroclastic rocks in the Pannonian basin. Front. Earth Sci. 9, 615768. https://doi.org/10.3389/feart.2021.615768.
Lukács, R., Harangi, Sz, Gál, P., Szepesi, J., Di Capua, A., Norini, G., Sulpizio, R., Groppelli, G., Fodor, L., 2022. Formal definition and description of lithostratigraphic units related to the Miocene silicic pyroclastic rocks outcropping in Northern Hungary: a revision. Geol. Carpath. 73 (2), 137–158. https://doi.org/10.31577/GeolCarp.73.2.3.
Maccaferri, F., Rivalta, E., Keir, D., Acocella, V., 2014. Off-rift volcanism in rift zones determined by crustal unloading. Nat. Geosci. 7, 297–300. https://doi.org/10.1038/ngeo2110.
Maccaferri, F., Rivalta, E., Passarelli, L., Aoki, Y., 2016. On the mechanisms governing dike arrest: Insight from the 2000 Miyakejima dike injection. Earth Planet. Sci. Lett. 434, 64–74. https://doi.org/10.1016/j.epsl.2015.11.024.
Márton, E., Fodor, L., 1995. Combination of palaeomagnetic and stress data—a case study from North Hungary. Tectonophysics 242, 99–114. https://doi.org/10.1016/0040-1951(94)00153-Z.
Márton, E., Márton, P., 1996. Large scale rotation in North Hungary during the Neogene as indicated by palaeomagnetic data. In: Morris, A., Tarling, D.H. (Eds.), Paleomagnetism and Tectonics of the Peri–Mediterranean Region, Geological Society London, Special Publications, 105, pp. 153–173.
Márton, E., Pécskay, Z., 1998. Complex evaluation of paleomagnetic and K/Ar isotope data of the Miocene ignimbritic volcanics in the Bükk Foreland, Hungary. Acta Geol. Hung. 41, 467–476.
Márton, E., Vass, D., Túnyi, I., Márton, P., Zelenka, T., 2007a. Paleomagnetic properties of the ignimbrites from the famous fossil footprints site, Ipolytarnóc (close to the Hungarian Slovak frontier) and their age assignment. Geol. Carpath. 58 (6), 531–540.
Márton, E., Zelenka, T., Márton, P., 2007b. Paleomagnetic correlation of Miocene pyroclastics of the Bükk Mts and their forelands. Central Eur. Geol. 50, 47–57. https://doi.org/10.1556/ceugeol.50.2007.1.4.
Mazzarini, F., Le Corvec, N., Isola, I., Favalli, M., 2016. Volcanic field elongation, vent distribution, and tectonic evolution of a continental rift: the Main Ethiopian Rift example. Geosphere 12, 706–720. https://doi.org/10.1130/GES01193.1.
Molnár, K., Lahitte, P., Dibacto, S., Benkó, Z., Agostini, S., Döncző, B., Ionescu, A., Milevski, I., Szikszai, Z., Kertész, Z., Temovski, M., 2022. The westernmost Late Miocene–Pliocene volcanic activity in the Vardar zone (North Macedonia). Int. J. Earth Sci. (Geologische Rundschau) 111, 749–766. https://doi.org/10.1007/s00531–021–02153–2.
Nemčok, M., Lexa, J., 1990. Evolution of the basin and range structure around the Žiar mountain range. Geol. Zbornik–Geologica Carpathica 41, 229–258.
Noszky, J., 1940. A Cserháthegység földtani viszonyai (Das Cserhát–Gebirge). Magyar tájak földtani leírása III. Geologische Beschreibung Ungarischer Landschaften III.
Oláh, P., Fodor, L., Tóth, T., Deák, A., Drijkoningen, G., Horváth, F., 2014. Geological results of the seismic surveys around Szentendre Island, Danube River, North Hungary. Földtani Közlöny 144 (4), 359–380.
Palotai, M., 2013. Oligocene−Miocene Tectonic Evolution of the Central Part of the Mid–Hungarian Shear Zone. PhD thesis, PhD School of Earth Sciences, Program for Geology and Geophysics. Eötvös Loránd University, Budapest, 147 p.

Palotai, M., Csontos, L., 2010. Strike-slip reactivation of a Paleogene to Miocene fold and thrust belt along the central part of the Mid-Hungarian Shear Zone. Geol. Carpath. 61 (6), 483–493. https://doi.org/10.2478/v10096-010-0030-3.

Pécskay, Z., Lexa, J., Szakács, A., Seghedi, I., Balogh, K., Konečny, V., Zelenka, T., Kovacs, M., Póka, T., Fulop, A., Márton, E., 2006. Geochronology of Neogene magmatism in the Carpathian arc and intra-Carpathian area. Geol. Carpath. 57 (6), 511–530.

Petrik, A.B., 2016. Structural Evolution of the Southern Bükk Foreland.. MSc thesis Dept. of Geology, Eötvös University, Budapest, 208 p.

Petrik, A., Beke, B., Fodor, L., Lukács, R., 2016. Cenozoic structural evolution of the southwestern Bükk Mts. and the southern part of the Darnó Deformation Belt (NE Hungary). Geol. Carpath. 67 (1), 83–104. https://doi.org/10.1515/geoca-2016-0005.

Pinel, V., Jaupart, C., 2004. Magma storage and horizontal dyke injection beneath a volcanic edifice. Earth Planet. Sci. Lett. 221, 245–262. https://doi.org/10.1016/S0012–821X(04)00076–7.

Plateaux, R., Béthoux, N., Bergerat, F., Mercier de Lépinay, B., 2014. Volcano–tectonic interactions revealed by inversion of focal mechanisms: stress field insight around and beneath the Vatnajökull ice cap in Iceland. Front. Earth Sci. 2, 9. https://doi.org/10.3389/feart.2014.00009.

Póka, T., Zelenka, T., Seghedi, I., Pécskay, Z., Márton, E., 2004. Miocene volcanism of the Cserhát Mts (N Hungary): Integrated volcano–tectonic, geochronologic and petrochemical study. Acta Geol. Hung. 47, 227–246. https://doi.org/10.1556/ageol.47.2004.2-3.7.

Pollard, D.D., 1987. Elementary fracture mechanics applied to the structural interpretation of dykes. In: Mafic Dyke Swarms, pp. 5–24.

Prakfalvi, P., Síkhegyi, F., Kaiser, M., 2005a. In: Gyalog, L. (Ed.), Geological Map of Hungary, 1:100000, Ballassagyarmat, M34–135. Geological Insitute of Hungary.

Prakfalvi, P., Síkhegyi, F., Kaiser, M., 2005b. In: Síkheygi, F., Gyalog, L. (Eds.), Geological Map of Hungary, 1:100000, Salgótarján, M34–136. Geological Insitute of Hungary.

Prakfalvi, P., Kuti, L., Síkhegyi, F., Kaiser, M., 2005c. In: Gyalog, L. (Ed.), Geological Map of Hungary, 1:100000, Vác L–34–3. Geological Insitute of Hungary.

Püspöki, Z., Hámor-Vidó, M., Pummer, T., Sári, K., Lendvay, P., Selmeczi, I., Detzky, G., Gúthy, T., Kiss, J., Kovács, Zs, Prakfalvi, P., McIntosh, R.W., Buday-Bódi, E., Báldi, K., Markos, G., 2017. A sequence stratigraphic investigation of a Miocene formation supported by coal seam quality parametres – Central Paratethys, N-Hungary. Int. J. Coal Geol. 179, 196–210. https://doi.org/10.1016/j.coal.2017.05.016.

Quidelleur, X., Gillot, P.-Y., Soler, V., Lefèvre, J.-C., 2001. K/Ar dating extended into the last millennium: application to the youngest effusive episode of the Teide Volcano (Spain). Geophys. Res. Lett. 28 (16), 3067–3070. https://doi.org/10.1029/2000GL012821.

Rivalta, E., Taisne, B., Bunger, A.P., Katz, R.F., 2015. A review of mechanical models of dike propagation: Schools of thought, results and future directions. Tectonophysics 638, 1–42. https://doi.org/10.1016/j.tecto.2014.10.003.

Rónai, A., Kuti, L., Pelikán, P., Kaiser, M., 2005. In: Gyalog, L. (Ed.), Geological Map of Hungary, 1:100000, Gyöngyös L–34–3. Geological Insitute of Hungary.

Ruch, J., Wang, T., Xu, W., Hensch, M., Jónsson, S., 2016. Oblique rift opening revealed by reoccurring magma injection in Central Iceland. Nat. Commun. 7, 12352. https://doi.org/10.1038/ncomms12352.

Ruszkiczay-Rüdiger, Zs, Fodor, L.I., Horváth, E., 2007. Neotectonics and Quaternary landscape evolution of the Gödöllő Hills, Central Pannonian Basin, Hungary. Glob. Planet. Chang. 58 (1–4), 181–196. https://doi.org/10.1016/j.gloplacha.2007.02.010.

Ruszkiczay-Rüdiger, Z., Fodor, L., Horváth, E., Telbisz, T., 2009. Discrimination of fluvial, eolian and neotectonic features in a low hilly landscape: a DEM-based morphotectonic analysis in the Central Pannonian Basin, Hungary. Geomorphology 104 (3–4), 203–217. https://doi.org/10.1016/j.geomorph.2008.08.014.

Schmiedel, T., Burchardt, S., Mattsson, T., Guldstrand, F., Galland, O., Palma, J.O., Skogby, H., 2021. Emplacement and segment geometry of large, high–viscosity magmatic sheets. Minerals 11, 1113. https://doi.org/10.3390/min11101113.

Schwarz, W.H., Trieloff, M., 2007. Intercalibration of Ar–40–Ar–39 age standards NL–25, HB3gr hornblende, GA1550, SB–3, HD–B1 biotite and BMus/2 muscovite. Chem. Geol. 242 (1–2), 218–231. https://doi.org/10.1016/j.chemgeo.2007.03.016.

Selmeczi, I., Fodor, L., Lukács, R., Szepesi, J., Sebe, K., Prakfalvi, P., Sztanó, O., 2024. Lower and Middle Miocene. In: Babinszki, E., Piros, O., Csillag, G., Fodor, L., Gyalog, L., Kercsmár, Z., Less, G., Lukács, R., Sebe, K., Selmeczi, I., Szepesi, J., Sztanó, O. (Eds.), Lithostratigraphic units of Hungary II. Cenozoic formations. SZTFH and Hungarian Academy of Sciences, Stratigraphic Subcommittee, Budapest, Hungary, pp. 52–107.

Shukla, G., Mallik, J., Mondal, P., 2022. Dimension-scaling relationships of Pachmarhi dyke swarm and their implications on Deccan magma emplacement. Tectonophysics 843, 229602. https://doi.org/10.1016/J.TECTO.2022.229602.

Sigmundsson, F., Hooper, A., Hreinsdóttir, S., Vogfjörd, K.S., Ófeigsson, B.G., Heimisson, E.R., Dumont, S., Parks, M., Spaans, K., Guðmundsson, G.B., 2015. Segmented lateral dyke growth in a rifting event at Bárðarbunga volcanic system, Iceland. Nature 517, 191–195. https://doi.org/10.1038/nature14111.

Sigmundsson, F., Parks, M., Hooper, A., Geirsson, H., Vogfjörd, K.S., Drouin, V., Ófeigsson, B.G., Hreinsdóttir, S., Hjaltadóttir, S., Jónsdóttir, K., Einarsson, P., Barsotti, S., Horálek, J., Ágústsdóttir, T., 2022. Deformation and seismicity decline before the 2021 Fagradalsfjall eruption. Nature 609, 523–528. https://doi.org/10.1038/s41586-022-05083-4.

Sigmundsson, F., Parks, M., Geirsson, H., Hooper, A., Drouin, V., Vogfjörd, K.S., Ófeigsson, B.G., Greiner, S.H., Yang, Y., Lanzi, C., De Pascale, G.P., 2024. Fracturing and tectonic stress drives ultrarapid magma flow into dikes. Science. https://doi.org/10.1126/science.adn2838 p.eadn2838.

Soós, B., 2017. A Zagyva–árok extenziójának szerkezete és mértéke.. MSc thesis Eötvös Loránd University, Budapest (in Hungarian).

Sóron, A.S., 2011. Paleoenvironmental and stratigraphic investigations of the foraminiferal fauna from the Karpatian (Lower Miocene) Garáb Schlier Formation of the Mátraverebély–122 (Mv–122) borehole (North Hungary). Central Eur. Geol. 54, 211–231. https://doi.org/10.1556/ceugeol.54.2011.3.1.

Spacapan, J.B., Galland, O., Leanza, H.A., Planke, S., 2016. Control of strike-slip fault on dyke emplacement and morphology. J. Geol. Soc. Lond. 173 (4), 573–576. https://doi.org/10.1144/jgs2015-166.

Steiger, R.H., Jäger, E., 1977. Subcommission on geochronology: convention on the use of decay constants in geo and cosmochronology. Earth Planet. Sci. Lett. 36 (3), 359–362. https://doi.org/10.1016/0012-821X(77)90060-7.

Stephens, T.L., Walker, R.J., Healy, D., Bubeck, A., England, R.W., 2018. Mechanical models to estimate the palaeostress state from igneous intrusions. J. Geophys. Solid Earth 9, 847–858. https://doi.org/10.5194/se-9-847-2018.

Sztanó, O., 1994. The tide-influenced Pétervására Sandstone, early Miocene, northern Hungary: Sedimentology, paleogeography and basin development. Geol. Ultraiect. 120, 1–155.

Sztanó, O., 1995. Palaeogeographic significance of tidal deposits: an example from an early Miocene Paratethys embayment, Northern Hungary. Palaeogeogr. Palaeoclimatol. Palaeoecol. 113, 173–187. https://doi.org/10.1016/0031-0182(95)00054-P.

Sztanó, O., Tari, G., 1993. Early Miocene basin evolution in northern Hungary: Tectonics and eustasy. Tectonophysics 226, 485–502. https://doi.org/10.1016/0040-1951(93)90134-6.

Tari, G., Horváth, F., Rumpler, J., 1992. Styles of extension in the Pannonian Basin. Tectonophysics 208, 203–219. https://doi.org/10.1016/b978-0-444-89912-5.50016-8.

Tari, G., Báldi, T., Báldi-Beke, M., 1993. Paleogene retroarc flexural basin beneath the Neogene Pannonian Basin: a geodynamical model. Tectonophysics 226, 433–455. https://doi.org/10.1016/0040–1951(93)90131–3.

Townsend, M., Pollard, D.D., Johnson, K., Culha, C., 2015. Jointing around magmatic dikes as a precursor to the development of volcanic plugs. Bull. Volcanol. 77, 1–13. https://doi.org/10.1007/s00445-015-0978-z.

Vass, D., Hók, J., Kováč, P., Elečko, M., 1993. The Paleogene and Neogene tectonic events of the Southern Slovakia depressions in the light of the stress-field analyses. Mineralia Slovaca 25, 79–92.

Vojtko, R., Klučiar, T., Králiková, S., Hók, J., Pelech, O., 2019. Late Badenian to Quaternary palaeostress evolution of the northeastern part of the Danube Basin and the southwestern slope of the Štiavnica Stratovolcano (Slovakia). Acta Geologica Slovaca 11, 15–29.

Walker, R.J., Healy, D., Kawanzaruwa, T.M., Wright, K.A., England, R.W., McCaffrey, K. J.W., Bubeck, A.A., Stephens, T.L., Farrell, N.J.C., Blenkinsop, T.G., 2017. Igneous sills as a record of horizontal shortening: the San Rafael subvolcanic field, Utah. GSA Bull. 129, 1052–1070. https://doi.org/10.1130/B31671.1.

Wein, Gy., 1977. Tectonics of the Buda Mts. Occasional Publications of the Geological Institute of Hungary, pp. 1–76.

Zelenka, T., Póka, T., Márton, E., Pécskay, Z., 2004. New data on stratigraphic position of the Tar Dacite Tuff Formation. In: Annual Report of the Geological Institute of Hungary from 2004, pp. 73–84.